

# A Re-Parameterized Vision Transformer (ReVT) for Domain-Generalized Semantic Segmentation

Jan-Aike Termöhlen    Timo Bartels    Tim Fingscheidt  
 Technische Universität Braunschweig, Germany  
 {j.termoehlen, timo.bartels, t.fingscheidt}@tu-bs.de

## Abstract

The task of semantic segmentation requires a model to assign semantic labels to each pixel of an image. However, the performance of such models degrades when deployed in an unseen domain with different data distributions compared to the training domain. We present a new augmentation-driven approach to domain generalization for semantic segmentation using a re-parameterized vision transformer (ReVT) with weight averaging of multiple models after training. We evaluate our approach on several benchmark datasets and achieve state-of-the-art mIoU performance of 47.3% (prior art: 46.3%) for small models and of 50.1% (prior art: 47.8%) for midsized models on commonly used benchmark datasets. At the same time, our method requires fewer parameters and reaches a higher frame rate than the best prior art. It is also easy to implement and, unlike network ensembles, does not add any computational complexity during inference.<sup>1</sup>

## 1. Introduction

Many methods for machine perception, e.g., for semantic segmentation, employ deep neural networks (DNNs) [11]. Due to the high labeling cost for semantic segmentation data, more and more synthetic data are used for training these DNNs. After training on the labeled (source) domain they should operate as robustly as possible in similar, but unseen (target) domains. However, this is often not the case since the data of the target domain differ from those of the training domain, leading to a so-called domain gap. There are many methods to deal with this domain gap that either require samples from the target domain during training [2, 3, 35], or alter the target data or the network parameters during inference [18, 19, 38]. An approach that does not have these drawbacks is domain generalization (DG). The aim of domain generalization is to train a network in a way that it generalizes well to unseen domains without

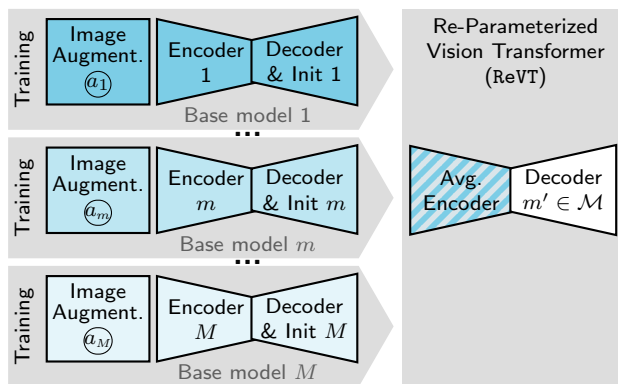


Figure 1. **High-level overview** of the generalization method. The set of all  $M$  base models trained on individual augmentations  $\mathcal{A}_m$  is denoted by  $\mathcal{M} = \{1, \dots, m, \dots, M\}$ . For the re-parameterized vision transformer (ReVT), any decoder  $m' \in \mathcal{M}$  can be used.

any adaptation steps. Although neural networks that employ vision transformer encoders currently achieve the best performance in segmentation tasks, modern DG methods are mostly presented with ResNet-based models, such as DeepLabv3+ [4] and FCN [23]. Due to its strong performance with a comparable or smaller number of parameters, we employ the transformer-based SegFormer [42] as the baseline for our domain generalization method.

A training or post-processing method that has proven itself in many applications is re-parameterization. Here, either individual layers, e.g., convolutional layers, or entire models trained with potentially different augmentations can be averaged to improve performance and generalization of the final model. The averaging can be performed either during training [15, 36] or after training [40, 41]. As sketched in Figure 1, in our work we advantageously combine the strengths of selected image augmentations [13, 39, 42] with the re-parameterization and show that this method leads to a significantly better generalization capability for transformer-based models. We also show that the method does not improve the performance of the commonly used ResNet-based models when trained with standard stochastic gradient descent (SGD), but that this can be

<sup>1</sup>Code is available at <https://github.com/ifnspaml/ReVT>

overcome by the use of the AdamW optimizer [24].

As shown in Figure 1, first,  $M$  base models are trained, with pre-trained encoders but different random decoder seeding, and potentially with dissimilar augmentations  $\mathcal{A}_m$ . Afterwards, the encoder networks can be averaged into one new encoder (re-parameterization), which extracts better generalizing features. This encoder can then be combined with any of the previously trained decoders and be used directly for segmentation.

Our contribution with this work is fourfold. First, we propose a re-parameterized vision transformer ReVT for domain-generalized semantic segmentation, resulting from  $M$  augmentation-individual base models. We achieve higher mIoU on unseen domains compared to methods that employ ResNet-based models, while requiring fewer parameters and achieving higher frame rates than the best prior art. Second, we analyze the effect of different network architectures, network parts, layer types, and optimizers on the re-parameterization. Third, we report on two more real datasets as common in the field and also going beyond customs in the field, we follow a stringent division of data splits into training, development, and test set. Finally, we set a new state-of-the-art benchmark on the synthetic-to-real domain generalization task for semantic segmentation.

## 2. Related Work

In this section, we discuss related works for our single-source domain generalization method. We start with the task of domain generalization, followed by related work on image augmentation and model re-parameterization.

### 2.1. Domain Generalization (DG)

In domain generalization for semantic segmentation, a model is trained on a set of labeled data from a specific (source) domain  $\mathcal{D}^S$  and then evaluated on new data from unseen (target) domains  $\mathcal{D}^T$ . The goal is to train a model that can generalize well to different domains and accurately segment new images. Following Qiao et al. [31], we distinguish between domain generalization and *single-source* domain generalization. The main difference between these two is that in the former, the model can be exposed to multiple domains during training, e.g., multiple labeled source domains or additional auxiliary domains. A dataset often used as an auxiliary domain is ImageNet [9], which is used to learn the style of real images [14,44]. In the *single-source* domain generalization task, the model is trained solely on one single domain.

Muandet et al. [25] proposed a so-called domain-invariant component analysis (DICA) minimizing the dissimilarity across domains during training. Liet al. [21] learn a domain-agnostic model on multiple domains via low-rank parameterized CNNs. Zhang et al. [47] employ meta-learning for domain generalization and an adaptation

of batch norm statistics in the target domain, and therefore present no pure DG method. Li et al. [22] propose an episodic training with a simple approach of aggregating data from multiple source domains for training. Yue et al. [44] first randomize the images with the style from real domains and then also enforce pyramid consistency between different styles. Their approach is not single-source domain, but requires an auxiliary domain for the style transfer. Huang et al. [14] follow a similar approach, but proposed to perform the domain randomization in the frequency domain of the images. Pan et al. [28] proposed a new instance-batch normalization (IBN) that is more robust w.r.t. appearance changes such as color shifts or brightness changes. Choi et al. [5] proposed an advanced loss that uses instance selective whitening. Peng et al. [30] proposed a network that includes semantic-aware normalization (SAN) as well as semantic-aware whitening (SAW). WildNet [20] employs feature stylization with styles from an auxiliary domain and enforces semantic consistency between the segmentation masks of stylized and original images and also between the segmentation masks of stylized images and the labels. Other than previous methods, that either perform checkpoint selection<sup>2</sup> [14,44] or hyperparameter tuning on evaluation data (official validation sets) of the target domains, we follow a stringent approach with distinct development sets for method design and hyperparameter tuning and perform no checkpoint selection (cf. Section 4.3). We also evaluate our approach on additional real domains, some of which represent strong domain shifts (cf. Section 4.1), and have not been explored by previous approaches.

### 2.2. Image Augmentation

Image augmentation techniques [8,12,13,27,45,46] aim at improving the performance of DNNs by increasing the variability of the training data. They reduce the risk of overfitting, e.g., to synthetic textures [17], and can improve the generalization capability of the model. Some recent augmentation methods mix full images [46], parts of images [45], specific class pixels [27], or combine the previously mentioned augmentation strategies with other image transformations [12,13]. We propose to use a number of  $M$  so-called base models with *individual* augmentations  $\mathcal{A}_m$  drawn from PixMix [13], bilateral filtering [39], and the baseline augmentations from the SegFormer method [42].

### 2.3. Model Re-Parameterization

The stochastic weight averaging (SWA) [15] method averages the network weights of the model during the training process with stochastic gradient descent (SGD) using a cyclical or constant learning rate. Similarly, Sämann et

<sup>2</sup>cf. <https://github.com/jxhuang0508/FSDR/issues/2#issuecomment-910089417>

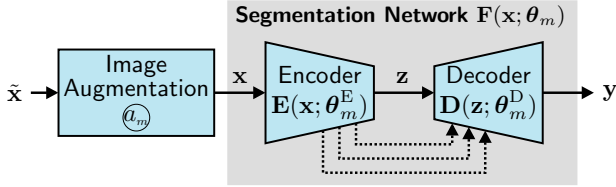


Figure 2. **Training setup** of base model  $m$  and notations. Dotted lines indicate skip connections.

al. [36] also employ the model averaging during training. A related method was also investigated by Kamp et al. [16] as an efficient decentralized learning protocol.

In contrast to methods that employ the re-parameterization during the training process [15, 36, 37], we adopt the re-parameterization approach by Wortsman et al. [41] that the authors dubbed “model soups” and performed the averaging of the model weights after various training processes. Note that it is also possible to re-parameterize specific layers and alter the architecture after re-parameterization, e.g., with RepVGG [10]. Wang et al. [40] analyzed these re-parameterization strategies for convolutional layers in different networks and proposed an advanced planned re-parameterized model.

### 3. Proposed Method

In this section, we will describe the mathematical notations and our new re-parameterized vision transformer (ReVT) training, including augmentations.

#### 3.1. Mathematical Notations

A high-level overview of the employed training setup is given in Figure 2. During training in the labeled source domain  $\mathcal{D}^S$ , an image  $\tilde{\mathbf{x}}$  is subject to augmentation methods and then denoted as  $\mathbf{x} \in \mathbb{G}^{H \times W \times C}$ , where  $\mathbb{G}$  denotes the set of integer gray values,  $H$  and  $W$  the image height and width in pixels, and  $C = 3$  the number of color channels. The augmented images  $\mathbf{x}$  are then transformed by the segmentation network  $\mathbf{F}$  with network parameters  $\boldsymbol{\theta}$  to obtain an output tensor  $\mathbf{y} = \mathbf{F}(\mathbf{x}; \boldsymbol{\theta}) = (y_{i,s}) \in \mathbb{I}^{H \times W \times S}$  that contains a pixel-wise posterior probability  $y_{i,s} = P(s|i, \mathbf{x})$  for all classes  $s \in \mathcal{S}$  at each pixel index  $i \in \mathcal{I} = \{1, 2, \dots, H \cdot W\}$ , with  $\mathbb{I} = [0, 1]$ . The segmentation network consists of an encoder  $\mathbf{z} = \mathbf{E}(\mathbf{x}; \boldsymbol{\theta}^E)$  and a decoder (segmentation head)  $\mathbf{y} = \mathbf{D}(\mathbf{z}; \boldsymbol{\theta}^D)$ , with the parameters  $\boldsymbol{\theta}^E$  and  $\boldsymbol{\theta}^D$ , respectively, resulting in  $\mathbf{y} = \mathbf{F}(\mathbf{x}; \boldsymbol{\theta}) = \mathbf{D}(\mathbf{E}(\mathbf{x}; \boldsymbol{\theta}^E); \boldsymbol{\theta}^D)$ . The number of parameters in a parameter tensor is denoted as  $|\boldsymbol{\theta}|$ . Different parameter tensors  $\boldsymbol{\theta}_m$  for the same architecture are marked by a subscript  $m \in \mathcal{M}$ , where  $\mathcal{M} = \{1, 2, \dots, M\}$  is the respective index set and  $M$  is the total number of models. The set of classes  $\mathcal{S} = \{1, 2, \dots, S\}$  contains the same  $S$  classes for source domain training and target domain inference (closed set). To

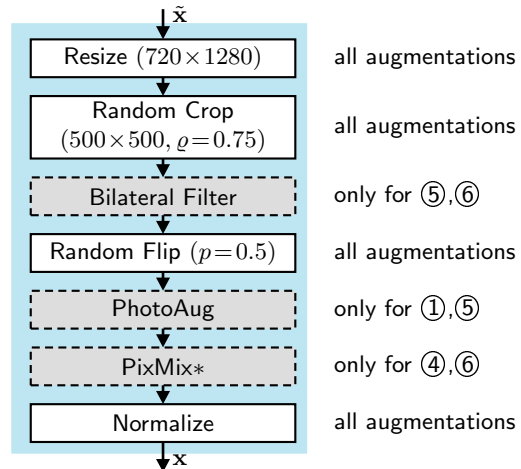


Figure 3. **Image augmentation pipeline** from Figures 1 and 2 employed during training. Use of blocks for augmentations @ noted at the side (cf. Section 4.2).

obtain the final classification map  $\mathbf{m} = (m_i) \in \mathcal{S}^{H \times W}$ , we compute  $m_i = \arg \max_{s \in \mathcal{S}} y_{i,s}$ .

#### 3.2. Re-Parameterized Vision Transformer (ReVT)

To the best of our knowledge we are the first to introduce vision transformer re-parameterization to domain generalization for semantic segmentation. In particular, each of the base models has seen an individual augmentation strategy in training. An illustrated overview of our proposed single-source domain generalization method for semantic segmentation is given in Figure 1. First,  $M$  segmentation networks of the same architecture are trained using ImageNet-pretrained encoders and different random decoder seeds and potentially also different augmentation strategies.

**Image augmentation:** The base model-individual augmentation steps employed during training are an important component of our method. We have illustrated the image augmentation pipeline in Figure 3. The baseline augmentation pipeline consists of resizing, random cropping, random flipping (Random Flip), photometric augmentation (PhotoAug), followed by a normalization to zero mean and unit variance. The bilateral filter [39] can be inserted before the random flipping (Figure 3, upper gray box). While PhotoAug is our default, it can optionally be replaced by the PixMix [13] algorithm (Figure 3, lower gray box). The original PixMix algorithm applies randomly selected augmentations. We employ the baseline augmentations (Random Flip + PhotoAug) here, which is why we refer to our PixMix variant as PixMix\*. All non-self-explanatory augmentations are explained in more detail in Supplement Section A. As a result of either different random seeding or augmentation, the network parameters will differ after training (Figure 1, left side).

**Re-parameterized vision transformer (ReVT):** After

Table 1. **Employed datasets.** The synthetic datasets GTA5 [32] and SYNTHIA [33] are used as (single) source domains ( $\mathcal{D}^S$ ). We employ various real-world datasets as target domains ( $\mathcal{D}^T$ ) to show the generalization capability of the proposed method.

Dataset Name	# Images in			
	$\mathcal{D}_{\text{full}}$	$\mathcal{D}_{\text{train}}$	$\mathcal{D}_{\text{dev}}$	$\mathcal{D}_{\text{test}*}$
GTA5 [32]	24,966	12,403	6,382	-
SYNTHIA [33] (SYN)	9,400	6,580	2,820	-
Cityscapes [7] (CS)	-	-	500	500
Mapillary Vistas [26] (MV)	-	-	-	2,000
BDD100k [43] (BDD)	-	-	-	1,000
ACDC [34]	-	-	-	406
KITTI [1] (KIT)	-	-	-	200

the training, the model weights  $\theta_m$ ,  $m \in \mathcal{M}$ , can be averaged resulting in  $\theta_\diamond$ . The new averaged model weights  $\theta_\diamond$  could be used during inference. Different to the method described by Sämann et al. [36], *we only re-parameterize the encoder weights*

$$\theta_\diamond^E = \frac{1}{M} \sum_{m \in \mathcal{M}} \theta_m^E, \quad (1)$$

resulting in our proposed ReVT as

$$\mathbf{y}^{\text{ReVT}} = (y_{i,s}^{\text{ReVT}}) = \mathbf{D}(\mathbf{E}^{\text{ReVT}}(\mathbf{x}; \theta_\diamond^E); \theta_{m'}^D), \quad (2)$$

with an arbitrarily chosen decoder  $m' \in \mathcal{M}$ .

## 4. Experimental Setup

In the following, we introduce the employed datasets and network architectures. Afterwards, we explain the training and evaluation settings, as well as the evaluation metrics. All architectures, procedures, and metrics are implemented using PyTorch [29] and the MMSegmentation toolbox [6].

### 4.1. Datasets

In our experiments we evaluate multiple established domain generalization benchmarks for semantic segmentation. The definition of the individual splits and their respective number of images is shown in Table 1. As our synthetic domains we employ GTA5 [32] and SYNTHIA [33]. We employ the three commonly used real-world datasets Cityscapes [7], BDD100k [43], and Mapillary Vistas [26] as target domains. Different to other publications, we also employ the ACDC [34] and the KITTI [1] datasets to provide more evidence of domain generalization on real domains. Particularly the ACDC dataset offers considerable benefit, since it includes images from four adverse conditions (fog, nighttime, rain, and snow), which are not present in the synthetic data. In DG benchmarks, there is no common practice

Table 2. Models and corresponding **number of parameters** for the full **segmentation networks** employed in this paper.

Segmentation Network	Encoder	$ \theta $ ( $\cdot 10^6$ )
DeepLabv3+ [4]	ResNet50	43.7
	ResNet101	62.7
SegFormer [42]	MiT-B2	27.4
	MiT-B3	47.2
	MiT-B5	84.7

on choosing which part of the synthetic dataset to use for training. Some publications use the entire GTA5 or SYNTHIA dataset for training [14, 44]. Other publications use the official training split of GTA5 and define their own training split for SYNTHIA [5, 20]. We follow Choi et al. [5] and employ their training and development split for SYNTHIA, and the official GTA5 training and validation set for training and development, respectively. Most DG methods base their design decisions on the official validation sets of the target domains and do not report test results. Since this approach is not rigorous, we follow an approach from domain adaptation [2] and sample 500 random images from the (unused) Cityscapes training set to be used as our development set, see Table 1. To allow comparison, we use the official validation sets of the real domains as test sets. To avoid confusion with the official (partly unpublished) test sets, we name our test sets “test\*”.

### 4.2. Network Architectures

For our experiments we employ two different network architectures that use an encoder-decoder structure, as illustrated in Figure 2. The employed segmentation networks and the corresponding number of parameters are listed in Table 2. First, we use a SegFormer [42] architecture with multiple skip connections from early layers to the decoder (SegFormer head). Second, a DeepLabv3+ [4] with only one skip connection from an early layer to the decoder is investigated. To ensure comparability with other reference methods, we will also perform experiments with several encoder sizes. If only SegFormer is mentioned and no additional information is given, this shall refer to the use of an MiT-B5 encoder. If only DeepLabv3+ is mentioned and no additional information is given, this shall refer to the use of a ResNet-101 encoder. For the re-parameterization of the models several encoders are required. As can be seen in Figure 1, the  $M$  models that are used in this process will be referred to as *base models* (not to be confused with baseline models, which are simply the standard SegFormer or DeepLabv3+ models), each with a potentially different image augmentation. The different image augmentations  $\mathcal{A}_m$  for each base model  $m$  are

Table 3. Performance (mIoU (%)), when **different network parts** are used in the **re-parameterization**. **Training** was performed on the **GTA5** ( $\mathcal{D}^S = \mathcal{D}_{\text{train}}^{\text{GTA5}}$ ) training set. **Evaluation** is performed on the **Cityscapes development set** ( $\mathcal{D}^T = \mathcal{D}_{\text{dev}}^{\text{CS}}$ ). Reported is the mean mIoU of  $\{\textcircled{1}, \textcircled{1}, \textcircled{1}\}$  models. For the re-parameterization, the mean is computed with one averaged encoder and the three associated decoders  $m \in \{1, 2, 3\}$ . Best results in bold face, second-best underlined.

Segmentation Network	Method: Re-Parameterization ...	mIoU (%) on $\mathcal{D}_{\text{dev}}^{\text{CS}}$
SegFormer (MiT-B5)	... not done (Baseline)	<u>44.3</u>
	... in encoder only	<b>47.5</b>
	... in decoder only	31.5
	... in full network	34.2
DeepLabv3+ (ResNet-101)	... not done (Baseline)	<b>34.7</b>
	... in encoder only	<u>31.9</u>
	... in decoder only	1.9
	... in full network	1.9

identified by  $\textcircled{1}$ ,  $\textcircled{2}$ , etc. If the same image augmentations is used multiple times, e.g.,  $\textcircled{1} = \textcircled{2} = \textcircled{3} = \textcircled{1}$ , then the  $M = 3$  base models were just trained with a different random seed. We then denote the used augmentations by  $\{\textcircled{1}, \textcircled{1}, \textcircled{1}\}$ .

### 4.3. Training, Evaluation, and Metrics

The hyperparameters for the image augmentation, training and evaluation (inference) procedures are provided in Supplement [Section B](#).

Unlike other methods [14, 44], we do not use the test\* sets (official validation sets) of the individual target domains for hyperparameter tuning or selection of training checkpoints. We train all our models for a fixed number of iterations and evaluate the checkpoint from the last iteration. We want to emphasize that we firmly believe that this is closer to a realistic deployment if a domain generalization method. To evaluate the methods, we employ the standard mean intersection over union (mIoU) of 19 segmentation classes [7, 32, 34]. Hyperparameter tuning is only based on our (self-defined) development sets  $\mathcal{D}_{\text{dev}}$ , see [Table 1](#). Specifically, we employ the mIoU mean on our out-of-domain (OOD) development sets for our design decisions on the proposed ReVT. To compare our method to other reference methods, we also report an mIoU over multiple domains. We follow Lee et al. [20] and Choi et al. [5] and evaluate the benchmark (BM) mean mIoU over the following benchmark set of data splits:  $\{\mathcal{D}_{\text{dev}}^{\text{GTA5}}, \mathcal{D}_{\text{dev}}^{\text{SYN}}, \mathcal{D}_{\text{test}^*}^{\text{CS}}, \mathcal{D}_{\text{test}^*}^{\text{BDD}}, \mathcal{D}_{\text{test}^*}^{\text{MV}}\}$ . We report the model size  $|\theta|$  and the frame rate in frames per second (fps), as measured on an NVIDIA A100 GPU.

Table 4. Performance (mIoU (%)) for different optimizer setups, i.e., optimizer, learning rate, weight decay, etc. We investigate the effect of the standard SegFormer optimizer setup (gray rows) and DeepLabv3+ optimizer setup (yellow rows) as shown in the Supplement [Section B](#), [Table 9](#). **Training** was performed on the full synthetic **GTA5** ( $\mathcal{D}^S = \mathcal{D}_{\text{train}}^{\text{GTA5}}$ ) dataset. Evaluation is performed on the **Cityscapes development set** ( $\mathcal{D}^T = \mathcal{D}_{\text{dev}}^{\text{CS}}$ ). Reported is the mean mIoU of  $\{\textcircled{1}, \textcircled{1}, \textcircled{1}\}$  models. Best results in bold face.

Network	Optimizer setup following ...	mIoU (%) on $\mathcal{D}_{\text{dev}}^{\text{CS}}$	
	(cf. <a href="#">Table 9</a> )	Baseline	re-parameterized
SegFormer	SegFormer	44.3	<b>47.5</b>
	DeepLabv3+	<b>46.2</b>	46.9
DeepLabv3+	SegFormer	<b>35.3</b>	<b>38.5</b>
	DeepLabv3+	34.7	31.9

## 5. Evaluation and Discussion

In this section, we will first investigate the basics of re-parameterization w.r.t. re-parameterized network parts, layers, and the number of base models. Afterwards, we evaluate different base model augmentations and optimizer methods during training to design our final ReVT. Finally, we compare our models to prior art DG methods.

### 5.1. Basic Investigations on Re-Parameterization

For the following experiments on basics of network re-parameterization, we only employ base models that were trained with the baseline image augmentation  $\textcircled{1}$ . If not stated otherwise, the experiments are performed with  $M = 3$  base models ( $\{\textcircled{1}, \textcircled{1}, \textcircled{1}\}$ ). Reported is always the mIoU on the Cityscapes development set ( $\mathcal{D}^T = \mathcal{D}_{\text{dev}}^{\text{CS}}$ ).

**Re-parameterized network parts:** In [Table 3](#) we investigate the effect of the re-parameterization, when applied to different network parts. We compare baseline models (no re-parameterization) and re-parameterization of the encoder only, the decoder only, and the full network. We show results for the SegFormer as well as for DeepLabv3+. It can be seen, that the encoder-only re-parameterization is the only setup which improves 3.2% absolute (abs.) over the baseline results from 44.3% to 47.5%. We also see that the DeepLabv3+ does not profit at all from any form of re-parameterization, actually, the performance even degrades from 34.7% to 31.9%. Therefore, in the remainder of the paper, we will use the re-parameterization for the vision transformer SegFormer to obtain the ReVT. We will also refer to the encoder-only re-parameterization simply as re-parameterization. In the following experiment we will further investigate why the DeepLabv3+ did not profit from

Table 5. Performance (mIoU (%)) of the SegFormer, when certain encoder **block or layer types** are used in the **re-parameterization**. Training was performed on the full synthetic GTA5 ( $\mathcal{D}^S = \mathcal{D}_{\text{train}}^{\text{GTA5}}$ ) dataset. Evaluation is performed on the Cityscapes development set ( $\mathcal{D}^T = \mathcal{D}_{\text{dev}}^{\text{CS}}$ ). Reported is the mean mIoU  $\pm$  the standard deviation of  $\{\textcircled{1}, \textcircled{1}, \textcircled{1}\}$  models. For the re-parameterization, the mean  $\pm$  standard deviation is computed with one averaged encoder and the three associated decoders  $m \in \{1, 2, 3\}$ . Best results in bold face, second-best underlined.

Method:	mIoU (%)
<b>Re-Parameterization ...</b>	<b>on <math>\mathcal{D}_{\text{dev}}^{\text{CS}}</math></b>
... not done (Baseline SegFormer)	44.3 $\pm$ 1.9
... in all blocks/layers	<b>47.5</b> $\pm$ 0.1
... in patch embedding blocks only	44.7 $\pm$ 1.7
... in attention blocks only	45.4 $\pm$ 1.1
... in Mix-FFN blocks only	<u>47.0</u> $\pm$ 0.6
... in convolutional layers only	45.1 $\pm$ 1.5
... in fully connected layers only	46.8 $\pm$ 0.6

re-parameterization and how this effect can be avoided.

**Optimizer choice:** In Table 4 we investigate the performance differences of baseline models and re-parameterized models when trained with different optimizer setups. The optimizer setup comprises all settings regarding the training process. We give a detailed list in Supplement Section B in Table 9. We test the effect of the standard optimizer setup for the SegFormer (AdamW, gray rows) and DeepLabv3+ (SGD, yellow rows). It can be seen that the SegFormer baseline is stronger when trained with the DeepLabv3+ setup (46.2% vs. 44.3%), but the gain from re-parameterization becomes significantly smaller (0.7% abs. improvement vs. 3.2% abs. improvement). For the DeepLabv3+, the SegFormer optimizer setup is the much better choice, because on the one hand the baseline has a better performance (35.3% vs. 34.7%), and on the other hand, it shows significant improvement (3.2% abs.) instead of deterioration (-2.8% abs.). For more analysis, see Supplement Section C.

**Re-parameterized blocks/layer types:** In Table 5 we investigate the performance of re-parameterization of different block and layer types within the SegFormer encoder. For each row, only the stated blocks or layers are re-parameterized, the rest of the models is kept the same for all  $m \in \mathcal{M}$ . The location of the specific blocks and layers is depicted in Supplement Section F. It can be seen in Table 5 that the method works best when all parameters of the encoder are used in the re-parameterization. The selection of specific blocks or layers does not bring any advantage. However, all independently evaluated layer / block types yield an improvement over the baseline.

**Number of base models:** In Figure 4 we show the performance of the re-parameterization vs. various ensembling

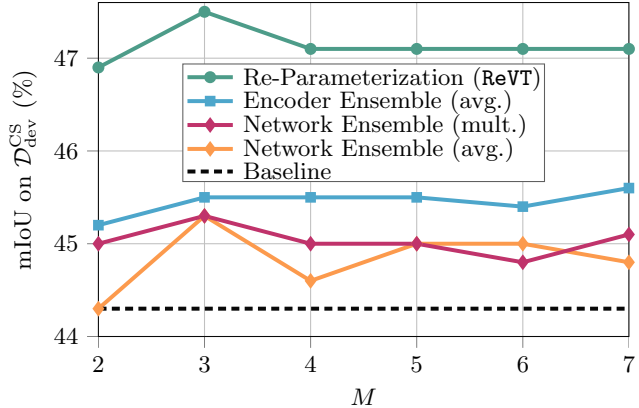


Figure 4. Performance (mIoU (%)) of the **re-parameterization** vs. **network/encoder ensembles** for different numbers  $M$  of base models. The **training** of the base models (SegFormer) was performed on the **GTA5** ( $\mathcal{D}^S = \mathcal{D}_{\text{train}}^{\text{GTA5}}$ ) dataset. The evaluation is performed on the **Cityscapes development set** ( $\mathcal{D}^T = \mathcal{D}_{\text{dev}}^{\text{CS}}$ ). The baseline mean is calculated from eight different models  $\textcircled{1}$ , and the re-parameterization from  $M$  models  $\textcircled{1}$ .

techniques for a different number  $M$  of models. For the ReVT (green), the mIoU is computed with an averaged encoder and all associated  $M$  decoders. For the encoder ensemble (blue), the feature maps  $\mathbf{z}$  from the encoders are averaged and then processed by all associated  $M$  decoders. For the network ensemble, the  $M$  output posteriors are averaged (orange) or multiplied (red). For  $M > 2$ , all methods consistently outperform the baseline (dashed line). In our case, three base models ( $M = 3$ ) provide the best results for the re-parameterization as well as for the network ensemble. The encoder ensemble on the other hand profits from a larger number of base models and yields the best performance for  $M = 7$ . The re-parameterization outperforms all ensembling techniques for all values of  $M$  by at least 1.5% abs. and for  $M = 3$  by at least 2.0% abs. It also comes with an  $M$ -fold lower computational complexity in inference.

## 5.2. ReVT Method Design

In Table 6 we evaluate various augmentation methods  $\textcircled{a}$  (see also Figure 3 and Supplement Section A) to identify strong base models. In the lower part of the table we report some ( $M = 3$ ) combinations  $\{\textcircled{1}, \textcircled{2}, \textcircled{3}\}$  of these base models by our re-parameterization. The gray columns indicate our development sets ( $\mathcal{D}_{\text{dev}}$ ), where the light gray column is  $\mathcal{D}_{\text{dev}}^{\text{GTA5}}$ . Since we train on  $\mathcal{D}_{\text{train}}^{\text{GTA5}}$ , we select our models on the (dark gray) OOD mean mIoU of  $\mathcal{D}_{\text{dev}}^{\text{SYN}}$  and  $\mathcal{D}_{\text{dev}}^{\text{CS}}$ . We select those base models for further evaluation in the ReVT that performed best, or second-, or third-ranked on the out-of-domain  $\mathcal{D}_{\text{dev}}^{\text{SYN}}$  and  $\mathcal{D}_{\text{dev}}^{\text{CS}}$  development sets (OOD mean). It can be seen that base models  $\textcircled{4}$ ,  $\textcircled{6}$ , and  $\textcircled{5}$  yield the best-, second-, third-ranked performance (41.0%, 40.7%, and 40.0%) on  $\mathcal{D}_{\text{dev}}^{\text{CS}}$  as well as  $\mathcal{D}_{\text{dev}}^{\text{SYN}}$  (out-of-domain data),

Table 6. Performance (mIoU (%)) of the SegFormer model (with an MiT-B5 encoder) using different domain generalization methods. **Training** was performed on the synthetic **GTA5** ( $\mathcal{D}^S = \mathcal{D}_{\text{train}}^{\text{GTA5}}$ ) dataset. **Evaluation** is performed on the **Cityscapes**, **GTA5**, and **SYNTHIA development sets** (gray columns) and on the **test\* data** of various real-world target datasets ( $\mathcal{D}^T = \mathcal{D}_{\text{test}*}$ ). Reported is the mean mIoU  $\pm$  the standard deviation of  $M = 3$  models with various image augmentations. For the ReVT, the mean  $\pm$  standard deviation is computed with one averaged encoder and the three associated decoders  $m \in \{1, 2, 3\}$ . Best results in bold face, second-best underlined.

Method performed:		mIoU (%) on							
		$\mathcal{D}_{\text{dev}}^{\text{GTA5}}$	$\mathcal{D}_{\text{dev}}^{\text{SYN}}$	$\mathcal{D}_{\text{dev}}^{\text{CS}}$	<b>OOD mean</b>	$\mathcal{D}_{\text{test}*}^{\text{CS}}$	$\mathcal{D}_{\text{test}*}^{\text{BDD}}$	$\mathcal{D}_{\text{test}*}^{\text{MV}}$	<b>test* mean</b>
during training	Baseline ①	68.2 $\pm$ 0.0	33.8 $\pm$ 0.7	44.3 $\pm$ 1.9	39.1 $\pm$ 5.4	45.3 $\pm$ 1.9	43.3 $\pm$ 1.3	46.8 $\pm$ 0.9	45.2 $\pm$ 2.0
	-PhotoAug ②	68.5 $\pm$ 0.1	32.3 $\pm$ 0.4	42.0 $\pm$ 1.1	37.2 $\pm$ 4.9	42.5 $\pm$ 1.5	42.3 $\pm$ 0.7	45.5 $\pm$ 0.9	43.4 $\pm$ 1.8
	-PhotoAug, -Rand. Flip ③	<b>69.0</b> $\pm$ 0.3	33.0 $\pm$ 0.5	42.8 $\pm$ 0.8	37.9 $\pm$ 4.9	42.3 $\pm$ 1.3	41.1 $\pm$ 0.8	46.4 $\pm$ 0.9	43.3 $\pm$ 2.5
	+PixMix* [13] ④	65.1 $\pm$ 0.2	<b>35.4</b> $\pm$ 1.1	<b>46.5</b> $\pm$ 0.3	<b>41.0</b> $\pm$ 5.6	46.9 $\pm$ 0.8	46.1 $\pm$ 1.0	51.2 $\pm$ 0.3	48.1 $\pm$ 2.4
	+Bilateral Filter (BF) [39] ⑤	68.0 $\pm$ 0.1	34.3 $\pm$ 0.6	45.7 $\pm$ 0.3	40.0 $\pm$ 5.7	46.8 $\pm$ 0.5	44.2 $\pm$ 1.1	49.4 $\pm$ 1.0	46.8 $\pm$ 2.3
	+PixMix* [13] +BF [39] ⑥	64.3 $\pm$ 0.1	35.2 $\pm$ 0.3	46.2 $\pm$ 0.7	40.7 $\pm$ 5.5	<b>47.5</b> $\pm$ 0.8	<b>46.7</b> $\pm$ 0.1	<b>51.5</b> $\pm$ 0.4	<b>48.6</b> $\pm$ 2.2
after training	ReVT {①,①,①}	68.6 $\pm$ 0.2	35.5 $\pm$ 0.4	47.5 $\pm$ 0.1	41.5 $\pm$ 6.0	49.3 $\pm$ 0.1	45.3 $\pm$ 0.5	49.3 $\pm$ 0.2	48.0 $\pm$ 1.9
	ReVT {②,②,②}	69.1 $\pm$ 0.1	34.1 $\pm$ 0.3	44.4 $\pm$ 0.5	39.3 $\pm$ 5.2	44.9 $\pm$ 0.5	44.1 $\pm$ 0.4	47.6 $\pm$ 0.4	45.5 $\pm$ 1.6
	ReVT {③,③,③}	<b>69.7</b> $\pm$ 0.1	35.0 $\pm$ 0.4	46.0 $\pm$ 0.3	40.5 $\pm$ 5.5	45.7 $\pm$ 0.2	43.5 $\pm$ 0.3	48.8 $\pm$ 0.2	46.0 $\pm$ 2.2
	ReVT {④,④,④}	65.7 $\pm$ 0.1	36.2 $\pm$ 0.0	<b>48.6</b> $\pm$ 0.3	42.4 $\pm$ 6.2	48.8 $\pm$ 0.3	47.5 $\pm$ 0.2	53.2 $\pm$ 0.3	49.8 $\pm$ 2.5
	ReVT {⑤,⑤,⑤}	68.5 $\pm$ 0.1	35.9 $\pm$ 0.0	47.3 $\pm$ 0.2	41.6 $\pm$ 5.7	48.6 $\pm$ 0.3	45.9 $\pm$ 0.2	51.2 $\pm$ 0.1	48.6 $\pm$ 2.2
	ReVT {⑥,⑥,⑥}	64.9 $\pm$ 0.0	36.1 $\pm$ 0.2	48.0 $\pm$ 0.2	42.1 $\pm$ 6.0	49.7 $\pm$ 0.2	<b>48.5</b> $\pm$ 0.4	<b>53.5</b> $\pm$ 0.1	<b>50.5</b> $\pm$ 2.1
	ReVT {④,⑤,⑥}	66.4 $\pm$ 0.7	36.9 $\pm$ 0.2	47.9 $\pm$ 0.5	42.4 $\pm$ 5.5	49.5 $\pm$ 0.4	48.1 $\pm$ 0.2	53.1 $\pm$ 0.2	50.2 $\pm$ 2.1
	ReVT {①,④,⑥}	66.4 $\pm$ 0.7	<b>37.3</b> $\pm$ 0.9	<b>48.6</b> $\pm$ 0.8	<b>42.9</b> $\pm$ 5.7	<b>50.0</b> $\pm$ 0.5	48.0 $\pm$ 0.3	52.8 $\pm$ 0.2	50.2 $\pm$ 2.0

whereas the base models ③ and ② yield the best and second-ranked performance (69.0% and 68.5%) on  $\mathcal{D}_{\text{dev}}^{\text{GTA5}}$  (in-domain data). This is to be expected, as the image augmentation makes it harder to learn in the source domain, but forces the base models to generalize slightly, as can be seen in the improved OOD performance of the base models ④, ⑤, and ⑥. In the following, we will report the performance for three different ReVTs. First, the ReVT {①,④,⑥} combines the baseline base model with the two best performing augmentation methods, which leads to the best mean OOD performance (42.9%). Second, the ReVT {④,⑤,⑥} combines the best-, second-, and third-ranked augmentation methods. Third, the ReVT {④,④,④} combines three base models with the single best augmentation method. The later two achieve the second-ranked performance on the OOD data (42.4%).

In the lower part of Table 6 it can be seen that the best test\* performance can be achieved with a ReVT {⑥,⑥,⑥} leading to a test\* mean performance of 50.5%. Our best dev set ReVT {①,④,⑥} achieves 50.2% as test\* mean.

### 5.3. Comparison to Prior Art DG Methods

In Table 7 we compare our method (ReVT) to prior art methods for domain generalization. We sort methods with respect to their encoder model (Enc.) and give the num-

ber of parameters of the full network in the third column. We also indicate whether the methods are trained with only one source domain, or if real auxiliary domains are employed and also report the inference frame rate. Methods are grouped to emphasize that w.r.t. the number of parameters  $|\theta|$  and w.r.t. the frame rate, the MiT-B2-based ReVT is competitive to ResNet-50-based methods (group 1), the MiT-B3-based ReVT is competitive to ResNet-101-based methods (group 2), while the MiT-B5-based ReVT builds an own group. Not all methods report the mIoU values for all datasets. In addition to the commonly used datasets, we also evaluate on ACDC [34] and KITTI [1] to provide more evidence of domain generalization on real domains.

It can be seen that *we exceed the performance of prior work that is comparable in network size*. In group 1, our ReVT with the MiT-B2 encoder achieves a benchmark mIoU (BM mean) of 47.29%, excelling the best prior work (WildNet with ResNet-50, 46.33%), while having fewer parameters (27.4 M vs. 43.7 M parameters) and a higher framerate (12 fps vs. 7.9 fps). In group 2, the ReVT with the MiT-B3 achieves a BM mean performance of 50.12%, which is 2.31% abs. higher than the best prior work (WildNet with ResNet-101, 47.81%), while having fewer parameters (47.2 M vs. 62.7 M) and a higher frame rate (10.7

Table 7. Performance (mIoU (%)) of various domain generalization methods employing different segmentation networks, sorted into three performance groups. **Training** was performed on the synthetic **GTA5** ( $\mathcal{D}^S = \mathcal{D}_{\text{train}}^{\text{GTA5}}$ ) dataset. The results marked with  $^\circ$  are cited from [20] and with  $*$  are cited from the respective paper. All results without any identifier are simulated. **Evaluation** is performed on the **SYNTHIA** and **GTA5 development sets** and on the **test\* data** of various real-world target datasets ( $\mathcal{D}^T = \mathcal{D}_{\text{test}*}$ ). BM means benchmark. For our simulations we report mean values over three runs with different seeding. Best performance per group in bold face, second best underlined.

Enc.	Method	$ \theta $ ( $\cdot 10^6$ )	Single Source	Frame Rate [fps]	mIoU (%) on								
					$\mathcal{D}_{\text{test}*}^{\text{CS}}$	$\mathcal{D}_{\text{test}*}^{\text{BDD}}$	$\mathcal{D}_{\text{test}*}^{\text{MV}}$	$\mathcal{D}_{\text{dev}}^{\text{SYN}}$	$\mathcal{D}_{\text{dev}}^{\text{GTA5}}$	$\mathcal{D}_{\text{test}*}^{\text{ACDC}}$	$\mathcal{D}_{\text{test}*}^{\text{KIT}}$	BM mean	
Group 1	ResNet-50	Baseline $^\circ$	43.7	✓	7.9	35.16	29.71	31.29	27.97	<u>71.17</u>	-	-	39.06
		IBN-Net $^\circ$ [28]	43.6	✓	8.4	36.52	34.18	38.74	30.41	70.78	-	-	42.12
		RobustNet $^\circ$ [5]	43.6	✓	8.5	38.78	35.64	40.38	28.97	70.16	-	-	42.78
		DRPC* [44]	49.6	✗	8.3	37.42	32.14	34.12	-	-	-	-	-
		SAN+SAW* [30]	25.6	✓	8.1	39.75	37.34	41.86	30.79	-	-	-	-
		WildNet $^\circ$ [20]	43.6	✗	7.9	44.62	38.42	46.09	31.34	<b>71.20</b>	-	-	46.33
Group 1	MiT-B2	Baseline	27.4	✓	<b>12.0</b>	41.73	38.77	44.15	31.20	65.95	30.20	44.34	44.36
		Ours: ReVT {④,④,④}	27.4	✓	<b>12.0</b>	45.06	40.44	49.46	<b>33.29</b>	62.57	<b>36.62</b>	<u>48.94</u>	46.16
		Ours: ReVT {④,⑤,⑥}	27.4	✓	<b>12.0</b>	<u>45.55</u>	<b>43.43</b>	<b>49.91</b>	<u>33.16</u>	63.58	36.66	49.27	<u>47.13</u>
		Ours: ReVT {①,④,⑥}	27.4	✓	<b>12.0</b>	<b>46.27</b>	<u>43.29</u>	<u>49.84</u>	<b>33.29</b>	63.74	<u>36.01</u>	<b>50.13</b>	<b>47.29</b>
Group 2	ResNet-101	Baseline $^\circ$	62.7	✓	5.1	35.73	34.06	33.42	29.06	<u>71.79</u>	-	-	40.81
		IBN-Net $^\circ$ [28]	62.6	✓	6.0	37.68	36.64	36.75	30.84	70.39	-	-	42.46
		RobustNet $^\circ$ [5]	62.6	✓	6.0	37.26	38.66	38.09	30.17	70.53	-	-	42.94
		DRPC* [44]	68.6	✗	5.3	42.53	38.72	38.05	-	-	-	-	-
		FSDR* [14]	68.6	✗	5.3	44.80	41.20	43.40	-	-	-	-	-
		SAN+SAW* [30]	44.6	✓	5.3	45.33	41.18	40.77	31.84	-	-	-	-
Group 2	WildNet $^\circ$ [20]	62.6	✗	5.1	45.79	41.73	47.08	32.51	<b>71.91</b>	-	-	47.81	
Group 2	MiT-B3	Baseline	47.2	✓	<b>10.7</b>	43.92	42.96	46.36	32.57	67.59	34.44	45.18	46.68
		Ours: ReVT {④,④,④}	47.2	✓	<b>10.7</b>	46.19	46.04	51.39	34.31	64.00	39.16	48.23	48.39
		Ours: ReVT {④,⑤,⑥}	47.2	✓	<b>10.7</b>	<u>47.95</u>	<b>48.26</b>	<b>52.59</b>	<b>36.80</b>	64.70	<u>40.96</u>	<b>49.84</b>	<u>50.06</u>
		Ours: ReVT {①,④,⑥}	47.2	✓	<b>10.7</b>	<b>48.33</b>	<u>48.17</u>	<u>52.28</u>	<u>36.67</u>	65.14	<b>41.38</b>	<u>49.74</u>	<b>50.12</b>
Group 3	MiT-B5	Baseline	84.7	✓	<b>9.7</b>	45.31	43.32	46.85	33.81	<b>68.17</b>	36.22	46.16	47.49
		Ours: ReVT {④,④,④}	84.7	✓	<b>9.7</b>	48.81	47.52	<b>53.21</b>	36.18	65.67	39.19	45.86	50.28
		Ours: ReVT {④,⑤,⑥}	84.7	✓	<b>9.7</b>	<u>49.55</u>	<b>48.11</b>	<u>53.06</u>	<u>36.86</u>	66.38	<u>40.36</u>	<u>46.88</u>	<u>50.79</u>
		Ours: ReVT {①,④,⑥}	84.7	✓	<b>9.7</b>	<b>49.96</b>	<u>48.01</u>	52.76	<b>37.27</b>	<u>66.40</u>	<b>41.15</b>	<b>50.39</b>	<b>50.88</b>

fps vs. 5 fps). In both groups, our method performs slightly worse in the source domain (GTA5), which is included in the BM mean, which, however, has little relevance for practical real-world applications.

It should also be noted, that our method does not employ any real auxiliary domains for image stylization such as WildNet [20], DRPC [44] and FSDR [14]. It can also be seen that our largest ReVT with an MiT-B5 encoder (group 3) achieves the overall highest performance of all evaluated models with a BM mean mIoU of 50.88%, still having a higher frame rate than ResNet-50-based WildNet [20], which achieves only a BM mean of 46.33%.

The higher mIoU values on the additional target domains (ACDC and KITTI) further indicate the excellent generalization capability of the ReVTs.

## 6. Conclusions

In this work we show how to improve the domain generalization capabilities of a vision transformer for semantic segmentation with a simple but effective augmentation and re-parameterization method (ReVT). We show the effect of different image augmentations and optimizer methods on the re-parameterization. Our method is smaller and computationally more efficient than network and encoder ensembles and also achieves state-of-the-art performance in the synthetic-to-real domain generalization task for semantic segmentation, exceeding prior art. In contrast to some prior art, our ReVT does not require an additional real auxiliary domain during training. We achieve a top mean mIoU of 50.88%, when using the largest model and also improve on the best prior art by 0.96% and 2.31% absolute using models with fewer parameters and a higher frame rate.



## References

- [1] Hassan Abu Alhaija, Siva Karthik Mustikovela, Lars Mescheder, Andreas Geiger, and Carsten Rother. Augmented Reality Meets Computer Vision: Efficient Data Generation for Urban Driving Scenes. *International Journal of Computer Vision*, 126(9):961–972, Sept. 2018. 4, 7
- [2] Nikita Araslanov and Stefan Roth. Self-Supervised Augmentation Consistency for Adapting Semantic Segmentation. In *Proc. of CVPR*, pages 15384–15394, virtual, June 2021. 1, 4
- [3] Jan-Aike Bolte, Markus Kamp, Antonia Breuer, Silviu Hmoceanu, Peter Schlicht, Fabian Hüger, Daniel Lipinski, and Tim Fingscheidt. Unsupervised Domain Adaptation to Improve Image Segmentation Quality Both in the Source and Target Domain. In *Proc. of CVPR - Workshops*, pages 1404–1413, Long Beach, CA, USA, June 2019. 1
- [4] Liang-Chieh Chen, Yukun Zhu, George Papandreou, Florian Schroff, and Hartwig Adam. Encoder-Decoder With Atrous Separable Convolution for Semantic Image Segmentation. In *Proc. of ECCV*, pages 801–818, Munich, Germany, Sept. 2018. 1, 4
- [5] Sungha Choi, Sanghun Jung, Huiwon Yun, Joanne T. Kim, Seungryong Kim, and Jaegul Choo. RobustNet: Improving Domain Generalization in Urban-Scene Segmentation via Instance Selective Whitening. In *Proc. of CVPR*, pages 11580–11590, virtual, June 2021. 2, 4, 5, 16
- [6] MMSegmentation Contributors. MMSegmentation: OpenMMLab Semantic Segmentation Toolbox and Benchmark. <https://github.com/open-mmlab/mms Segmentation>, 2020. 4
- [7] Marius Cordts, Mohamed Omran, Sebastian Ramos, Timo Rehfeld, Markus Enzweiler, Rodrigo Benenson, Uwe Franke, Stefan Roth, and Bernt Schiele. The Cityscapes Dataset for Semantic Urban Scene Understanding. In *Proc. of CVPR*, pages 3213–3223, Las Vegas, NV, USA, June 2016. 4, 5
- [8] Ekin D. Cubuk, Barret Zoph, Dandelion Mane, Vijay Vasudevan, and Quoc V. Le. AutoAugment: Learning Augmentation Strategies From Data. In *Proc. of CVPR*, pages 113–123, Long Beach, CA, USA, June 2019. 2
- [9] Jia Deng, Wei Dong, Richard Socher, Li-Jia Li, Kai Li, and Li Fei-Fei. ImageNet: A Large-Scale Hierarchical Image Database. In *Proc. of CVPR*, pages 248–255, Miami, FL, USA, June 2009. 2
- [10] Xiaohan Ding, Xiangyu Zhang, Ningning Ma, Jungong Han, Guiguang Ding, and Jian Sun. RepVGG: Making VGG-Style ConvNets Great Again. In *Proc. of CVPR*, pages 13733–13742, virtual, June 2021. 3
- [11] Tim Fingscheidt, Hanno Gottschalk, and Sebastian Houben, editors. *Deep Neural Networks and Data for Automated Driving: Robustness, Uncertainty Quantification, and Insights Towards Safety*. Springer Nature, Cham, 2022. 1
- [12] Dan Hendrycks, Norman Mu, Ekin Dogus Cubuk, Barret Zoph, Justin Gilmer, and Balaji Lakshminarayanan. AugMix: A Simple Data Processing Method to Improve Robustness and Uncertainty. In *Proc. of ICLR*, pages 1–15, virtual, Apr. 2020. 2
- [13] Dan Hendrycks, Andy Zou, Mantas Mazeika, Leonard Tang, Bo Li, Dawn Song, and Jacob Steinhardt. PixMix: Dream-like Pictures Comprehensively Improve Safety Measures. In *Proc. of CVPR*, pages 16783–16792, New Orleans, LA, USA, June 2022. 1, 2, 3, 11
- [14] Jiaying Huang, Dayan Guan, Aoran Xiao, and Shijian Lu. FSDR: Frequency Space Domain Randomization for Domain Generalization. In *Proc. of CVPR*, pages 6891–6902, virtual, June 2021. 2, 4, 5, 8, 16
- [15] Pavel Izmailov, Dmitrii Podoprikin, Timur Garipov, Dmitry P. Vetrov, and Andrew Gordon Wilson. Averaging Weights Leads to Wider Optima and Better Generalization. In *Proc. of UAI*, pages 1–10, Monterey, CA, USA, Aug. 2018. 1, 2, 3
- [16] Michael Kamp, Linara Adilova, Joachim Sicking, Fabian Hüger, Peter Schlicht, Tim Wirtz, and Stefan Wrobel. Efficient Decentralized Deep Learning by Dynamic Model Averaging. In *Proc. of ECML PKDD*, pages 7393–4090, Dublin, Ireland, Sept. 2018. 3
- [17] Myeongjin Kim and Hyeran Byun. Learning Texture Invariant Representation for Domain Adaptation of Semantic Segmentation. In *Proc. of CVPR*, pages 12975–12984, Seattle, WA, USA, June 2020. 2
- [18] Marvin Klingner, Mouadh Ayache, and Tim Fingscheidt. Continual BatchNorm Adaptation (CBNA) for Semantic Segmentation. *IEEE Transactions on Intelligent Transportation Systems*, 23(11):20899–20911, 2022. 1
- [19] Marvin Klingner, Jan-Aike Termöhlen, Jacob Ritterbach, and Tim Fingscheidt. Unsupervised BatchNorm Adaptation (UBNA): A Domain Adaptation Method for Semantic Segmentation Without Using Source Domain Representations. In *Proc. of WACV - Workshops*, pages 210–220, Waikoloa, HI, USA, Jan. 2022. 1, 15, 16
- [20] Suhyeon Lee, Hongje Seong, Seongwon Lee, and Euntai Kim. WildNet: Learning Domain Generalized Semantic Segmentation from the Wild. In *Proc. of CVPR*, pages 9936–9946, New Orleans, LA, USA, June 2022. 2, 4, 5, 8, 16
- [21] Da Li, Yongxin Yang, Yi-Zhe Song, and Timothy M. Hospedales. Deeper, Broader and Artier Domain Generalization. In *Proc. of ICCV*, pages 5542–5550, Venice, Italy, Oct. 2017. 2
- [22] Da Li, Jianshu Zhang, Yongxin Yang, Cong Liu, Yi-Zhe Song, and Timothy M. Hospedales. Episodic Training for Domain Generalization. In *Proc. of ICCV*, pages 1446–1455, Seoul, Korea, Oct. 2019. 2
- [23] Jonathan Long, Evan Shelhamer, and Trevor Darrell. Fully Convolutional Networks for Semantic Segmentation. In *Proc. of CVPR*, pages 3431–3440, Boston, MA, USA, June 2015. 1
- [24] Ilya Loshchilov and Frank Hutter. Decoupled Weight Decay Regularization. In *Proc. of ICLR*, pages 1–18, New Orleans, LA, USA, May 2019. 2, 13
- [25] Krikamol Muandet, David Balduzzi, and Bernhard Schölkopf. Domain Generalization via Invariant Feature Representation. In *Proc. of ICML*, pages 10–18, Atlanta, GA, USA, June 2013. 2

- [26] Gerhard Neuhold, Tobias Ollmann, Samuel Rota Bulò, and Peter Kotschieder. The Mapillary Vistas Dataset for Semantic Understanding of Street Scenes. In *Proc. of ICCV*, pages 4990–4999, Venice, Italy, Oct. 2017. [4](#)
- [27] Viktor Olsson, Wilhelm Tranheden, Juliano Pinto, and Lennart Svensson. ClassMix: Segmentation-Based Data Augmentation for Semi-Supervised Learning. In *Proc. of WACV*, pages 1369–1378, Jan. 2021. [2](#)
- [28] Xingang Pan, Ping Luo, Jianping Shi, and Xiaoou Tang. Two at Once: Enhancing Learning and Generalization Capacities via IBN-Net. In *Proc. of ECCV*, pages 464–479, Munich, Germany, Sept. 2018. [2](#)
- [29] Adam Paszke, Sam Gross, Francisco Massa, Adam Lerer, James Bradbury, Gregory Chanan, Trevor Killeen, Zeming Lin, Natalia Gimelshein, Luca Antiga, Alban Desmaison, et al. PyTorch: An Imperative Style, High-Performance Deep Learning Library. In *Proc. of NeurIPS*, pages 8024–8035, Vancouver, BC, Canada, Dec. 2019. [4](#)
- [30] Duo Peng, Yinjie Lei, Munawar Hayat, Yulan Guo, and Wen Li. Semantic-Aware Domain Generalized Segmentation. In *Proc. of CVPR*, pages 2594–2605, New Orleans, LA, USA, June 2022. [2](#), [15](#), [16](#)
- [31] Fengchun Qiao, Long Zhao, and xi Peng. Learning to Learn Single Domain Generalization. In *Proc. of CVPR*, pages 12556–12565, virtual, June 2020. [2](#)
- [32] Stephan Richter, Vibhav Vineet, Stefan Roth, and Vladlen Koltun. Playing for Data: Ground Truth from Computer Games. In *Proc. of ECCV*, pages 102–118, Amsterdam, Netherlands, Oct. 2016. [4](#), [5](#)
- [33] German Ros, Laura Sellart, Joanna Materzynska, David Vazquez, and Antonio M. Lopez. The SYNTHIA Dataset: A Large Collection of Synthetic Images for Semantic Segmentation of Urban Scenes. In *Proc. of CVPR*, pages 3234–3243, Las Vegas, NV, USA, June 2016. [4](#)
- [34] Christos Sakaridis, Dengxin Dai, and Luc Van Gool. ACDC: The Adverse Conditions Dataset with Correspondences for Semantic Driving Scene Understanding. In *Proc. of ICCV*, pages 10765–10775, virtual, Oct. 2021. [4](#), [5](#), [7](#)
- [35] Manuel Schwonberg, Joshua Niemeijer, Jan-Aike Termöhlen, Jörg P. Schäfer, Nico M. Schmidt, Hanno Gottschalk, and Tim Fingscheidt. Survey on Unsupervised Domain Adaptation for Semantic Segmentation for Visual Perception in Automated Driving. *IEEE Access*, 11:54296–54336, 2023. [1](#)
- [36] Timo Sämann, Ahmed Mostafa Hammam, Andrei Bursuc, Christoph Stiller, and Horst-Michael Groß. Improving Predictive Performance and Calibration by Weight Fusion in Semantic Segmentation. *arXiv:2207.11211*, July 2022. [1](#), [3](#), [4](#)
- [37] Antti Tarvainen and Harri Valpola. Mean Teachers are Better Role Models: Weight-Averaged Consistency Targets Improve Semi-Supervised Deep Learning Results. In *Proc. of NIPS*, pages 1–10, Long Beach, CA, USA, Dec. 2017. [3](#)
- [38] Jan-Aike Termöhlen, Marvin Klingner, Leon J. Brettin, Nico M. Schmidt, and Tim Fingscheidt. Continual Unsupervised Domain Adaptation for Semantic Segmentation by Online Frequency Domain Style Transfer. In *Proc. of ITSC*, pages 2881–2888, virtual, Sept. 2021. [1](#)
- [39] Carlo Tomasi and Roberto Manduchi. Bilateral Filtering for Fray and Color Images. In *Proc. of ICCV*, pages 839–846, Bombay, India, Jan. 1998. [1](#), [2](#), [3](#)
- [40] Chien-Yao Wang, Alexey Bochkovskiy, and Hong-Yuan Mark Liao. YOLOv7: Trainable Bag-of-Freebies Sets New State-of-the-Art for Real-Time Object Detectors, July 2022. [1](#), [3](#)
- [41] Mitchell Wortsman, Gabriel Ilharco, Samir Ya Gadre, Rebecca Roelofs, Raphael Gontijo-Lopes, Ari S Morcos, Hongseok Namkoong, Ali Farhadi, Yair Carmon, Simon Kornblith, and Ludwig Schmidt. Model Soups: Averaging Weights of Multiple Fine-Tuned Models Improves Accuracy Without Increasing Inference Time. In *Proc. of ICML*, pages 23965–23998, Baltimore, MD, USA, July 2022. [1](#), [3](#)
- [42] Enze Xie, Wenhai Wang, Zhiding Yu, Anima Anandkumar, Jose M. Alvarez, and Ping Luo. SegFormer: Simple and Efficient Design for Semantic Segmentation with Transformers. In *Proc. of NeurIPS*, pages 12077–12090, virtual, Dec. 2021. [1](#), [2](#), [4](#)
- [43] Fisher Yu, Wenqi Xian, Yingying Chen, Fangchen Liu, Mike Liao, Vashisht Madhavan, and Trevor Darrell. BDD100K: A Diverse Driving Video Database With Scalable Annotation Tooling. *arXiv*, (1805.04687), Aug. 2018. [4](#)
- [44] Xiangyu Yue, Yang Zhang, Sicheng Zhao, Alberto Sangiovanni-Vincentelli, Kurt Keutzer, and Boqing Gong. Domain Randomization and Pyramid Consistency: Simulation-to-Real Generalization Without Accessing Target Domain Data. In *Proc. of ICCV*, pages 2100–2110, Seoul, Korea, Oct. 2019. [2](#), [4](#), [5](#), [8](#), [16](#)
- [45] Sangdoon Yun, Dongyoon Han, Seong Joon Oh, Sanghyuk Chun, Junsuk Choe, and Youngjoon Yoo. CutMix: Regularization Strategy to Train Strong Classifiers With Localizable Features. In *Proc. of ICCV*, pages 6023–6032, Seoul, Korea, Oct. 2019. [2](#)
- [46] Hongyi Zhang, Moustapha Cisse, Yann N. Dauphin, and David Lopez-Paz. mixup: Beyond Empirical Risk Minimization. In *Proc. of ICLR*, pages 113–123, Vancouver, Canada, Apr. 2018. [2](#)
- [47] Jian Zhang, Lei Qi, Yinghuan Shi, and Yang Gao. Generalizable Semantic Segmentation via Model-Agnostic Learning and Target-Specific Normalization. *arXiv*, (2003.12296), May 2020. [2](#)

## Supplementary Material

In this supplementary material we give a detailed overview of the training and evaluation settings along with hyperparameters. We also provide a detailed description of the employed augmentation methods. Further, we show additional ablation studies and investigations. We also depict the SegFormer architecture in a block diagram. Finally, we discuss limitations and ethical implications for our method.

### A. Detailed Description of Augmentation Methods

In the following section, we present a detailed description of the employed augmentation methods.

**Random crop:** Parameter  $\varrho$  defines the maximum proportion a single class can occupy in the random crop.

**PhotoAug:** Photometric augmentation (PhotoAug) comprises the following steps: Each transformation is applied to the image with a probability of 0.5. The position of the random contrast adjustment is in second (mode ❶) or second to last position (mode ❷). The position is randomly selected for each image.

1. random brightness
2. if ❶: random contrast
3. convert color from RGB to HSV
4. random saturation
5. random hue
6. convert color from HSV to RGB
7. if ❷: random contrast
8. randomly swap channels

**Bilateral filter:** A bilateral filter smoothes an image while preserving sharp edges. Its focus is on the removal of noise and textures. In general, it is a Gaussian filter that smoothes less in non-uniform regions (edge regions) and more in uniform image regions (non-edge regions). The bilateral filter at pixel index  $i$  can be described as:

$$G(i) = \frac{1}{w} \sum_{j \in \mathcal{J}} N(\Delta_{ij}; \sigma_s^2) N(\|\mathbf{x}_i - \mathbf{x}_j\|_2; \sigma_c^2) \mathbf{x}_j, \quad (3)$$

with

$$N(d; \sigma^2) = e^{-\frac{1}{2}(\frac{d}{\sigma})^2}, \quad (4)$$

and normalizing factor

$$w = \sum_{j \in \mathcal{J}} N(\Delta_{ij}; \sigma_s^2) N(\|\mathbf{x}_i - \mathbf{x}_j\|_2; \sigma_c^2). \quad (5)$$

The neighboring pixel index is denoted as  $j$  and stems from the neighborhood  $\mathcal{J}$ . The neighborhood is defined by the kernel size which we sample from a uniform distribution between 1 (px) and 15 (px). Distances  $\Delta_{ij} = \sqrt{|h_i - h_j|^2 + |w_i - w_j|^2}$  and  $\|\mathbf{x}_i - \mathbf{x}_j\|_2$  denote the (Euclidean) pixel distance and color difference, respectively,

Listing 1. Pseudo-code of the PixMix [13] data augmentation.

```
def PixMix(x, z, K, beta): # mixing image z in Z
    x0 = random.choice({augment(x), x})
    # random number of mixing rounds
    for k = 1: random.choice({0, 1, ..., K}):
        xmix = random.choice({augment(x), z})
        mix_op = random.choice({add, multiply})
        xk = mix_op(xk-1, xmix, beta)
    return xk
```

where  $h_i$  and  $w_i$  are the height and width position of pixel  $i$  and  $\mathbf{x}_i \in \mathbb{G}^3$  denotes the vector of RGB values for pixel  $i$  (likewise for pixel  $j$ ). We set the spatial distance to  $\sigma_s = 75$  and the color distance to  $\sigma_c = 75$ . The probability for applying this filter is set to  $p = 0.5$ .

**PixMix:** The PixMix [13] augmentation method comprises multiple processing steps as shown in Listing 1. Here,  $\mathbf{x}$  denotes the input image and  $\mathbf{z} \in \mathcal{Z}$  denotes the mixing image from the PixMix set of fractal images  $\mathcal{Z}$  [13]. We set the maximum number of mixing rounds to  $K = 3$ . Note that the for loop is not executed for random choice = 0. The **mix\_op**( $\cdot$ ) function is randomly chosen to be either addition (**add**) or multiplication (**multiply**). It gets the images  $\tilde{\mathbf{x}}_{k-1}$  and  $\tilde{\mathbf{x}}_{\text{mix}}$  as inputs, as well as  $\beta = 3$ , which is used to generate independent weighting factors for the images. The weighting factors are sampled from a Beta distribution. For the **augment**( $\cdot$ ) function in the PixMix pseudocode we used only baseline augmentation methods PhotoAug and Random Flip (cf. Figure 3), that is why we denote the method as PixMix\*.

### B. Training/Evaluation Settings, Hyperparameters

In the following section, we will provide a detailed overview of the training and evaluation settings and hyperparameters. For the training and evaluation we employ PyTorch v.3.8.13 and the MMSegmentation toolbox v.0.11.0. Additionally, we refer to our repository, where all code for the conducted experiments is made available<sup>3</sup>.

**Training phase:** In Table 9 we list all settings and hyperparameters that were used for the training process. The polynomial learning rate schedule is defined as follows:

$$\eta(\tau) = \eta_0 \left(1 - \frac{\tau}{\tau_{\text{max}}}\right)^{0.9}, \quad (6)$$

with  $\eta(\tau)$  being the learning rate at optimizer step (iteration)  $\tau$  and  $\eta_0$  being the initial learning rate. The maximum number of iterations is given by  $\tau_{\text{max}}$ .

During training, the images from the source domain  $\mathcal{D}^S$  get resized to a resolution of  $720 \times 1280$ .

**Evaluation phase:** For evaluation, we always employ the final model weights after the full training and do not perform any checkpoint selection. We resize the input images

<sup>3</sup>Code is available at <https://github.com/ifnspaml/ReVT>

Table 9. **Settings and hyperparameters** for the SegFormer and DeepLabv3+ training.

Setting / Hyperparameter	SegFormer	DeepLabv3+
Optimizer	AdamW [24]	SGD
# of training iterations ( $\tau_{\max}$ )	40,000	60,000
Momentum values (AdamW) ( $\beta_1, \beta_2$ )	0.9, 0.999	-
Momentum ( $\beta$ )	-	0.9
Warm-up iterations	1500	-
Warm-up ratio	$1 \cdot 10^{-6}$	-
Initial LR ( $\eta_0$ )	$6 \cdot 10^{-5}$	$1 \cdot 10^{-3}$
Weight decay $\omega$	0.01	0.0005
Learning rate (LR) schedule ( $\eta(\tau)$ )	Polynomial (6)	Polynomial (6)
Batch size	2	2
Random decoder init	Kaiming initialization	Kaiming initialization
Resized input resolution $\mathcal{D}_{\text{train}}^{\text{GTA5}}$	$720 \times 1280$	$720 \times 1280$

Table 8. **Image and label resolution** [ $\text{px} \times \text{px}$ ] for the employed **evaluation** datasets. <sup>o</sup>In both GTA and KITTI, there are images that differ by a few pixels from their normal resolution. <sup>\*</sup>The crowd-sourced Mapillary Vistas dataset does not have a fixed resolution, but a highly variable one.

Dataset name	Resolution ( $H \times W$ ) of ...	
	resized images	labels
GTA5 [32]	$512 \times 932^{\circ}$	$1052 \times 1914^{\circ}$
SYNTHIA [33] (SYN)	$512 \times 862$	$760 \times 1280$
Cityscapes [7] (CS)	$512 \times 1024$	$1024 \times 2048$
Mapillary Vistas [26] (MV)	various*	various*
BDD100k [43] (BDD)	$512 \times 910$	$720 \times 1280$
ACDC [34]	$512 \times 910$	$1080 \times 1920$
KITTI [1] (KIT)	$309 \times 1024^{\circ}$	$375 \times 1242^{\circ}$

during evaluation in a way that the image will be rescaled as large as possible within a pre-defined scale ( $512 \times 1024$ ), while still keeping their aspect ratios. The network output is then resized to the original image resolution. The mIoU is calculated on the original resolution, also referred to as label resolution. The resized image and the original label resolutions for all employed datasets are listed in Table 8.

The frame rate computations were performed on the rescaled Cityscapes dataset. We used 200 images for inference and computed the mean frame rate after a warmup phase of five images to account for any delays due to image reading operations.

### C. Additional Details on the Choice of Optimizer

In our experiments in Table 4 we show that the choice of optimizer has a strong effect on the baseline perfor-

mance of the models, as well as on the performance after re-parameterization. In Figure 5, we compare the SegFormer architecture with its standard optimizer setup (left) and the DeepLabv3+ architecture with its standard optimizer setup (right). We show the mean cosine similarity between three baseline ( $\textcircled{1}$ ) models for the encoder only ( $\theta^E$ , upper plots) and the full model ( $\theta$ , center plots), during the training process. Note that the standard number of iterations differs for both models and is 40,000 for the SegFormer and 60,000 for the DeepLabv3+.

It can be seen that the mean cosine similarity for the network parts that are re-parameterized in our method (encoder only) have a similar mean cosine similarity after the training for both networks (0.995). In the bottom plots of the figure, we report the mIoU values for both in-domain (GTA5, green) and out-of-domain (OOD) data (Cityscapes, red) for the baseline (dashed lines) and re-parameterized (solid lines) models. It can be seen that the performance of the re-parameterized models is higher for the SegFormer for any training iteration. For the DeepLabv3+, however, the baseline performance is always higher for in-domain data (green) and fluctuates for OOD data (red), but ultimately the baseline performance is also higher for OOD data in the last iterations.

Since the mean cosine similarity did not provide any insights into the causes for the poor performance of the re-parameterized DeepLabv3+, we further investigated the mean cosine similarity for individual layers  $\ell$  of the networks as shown in Figure 6. We show the layer-wise mean cosine similarity for the encoder network ( $\theta_{\ell}^E$ ), where  $\ell$  indicates the layer index. For the purpose of clarity, we only mark the first layer of each of the major network blocks. For the SegFormer, we indicate the transformer blocks by  $Bb$  with  $b$  being the block index (cf. Fig-

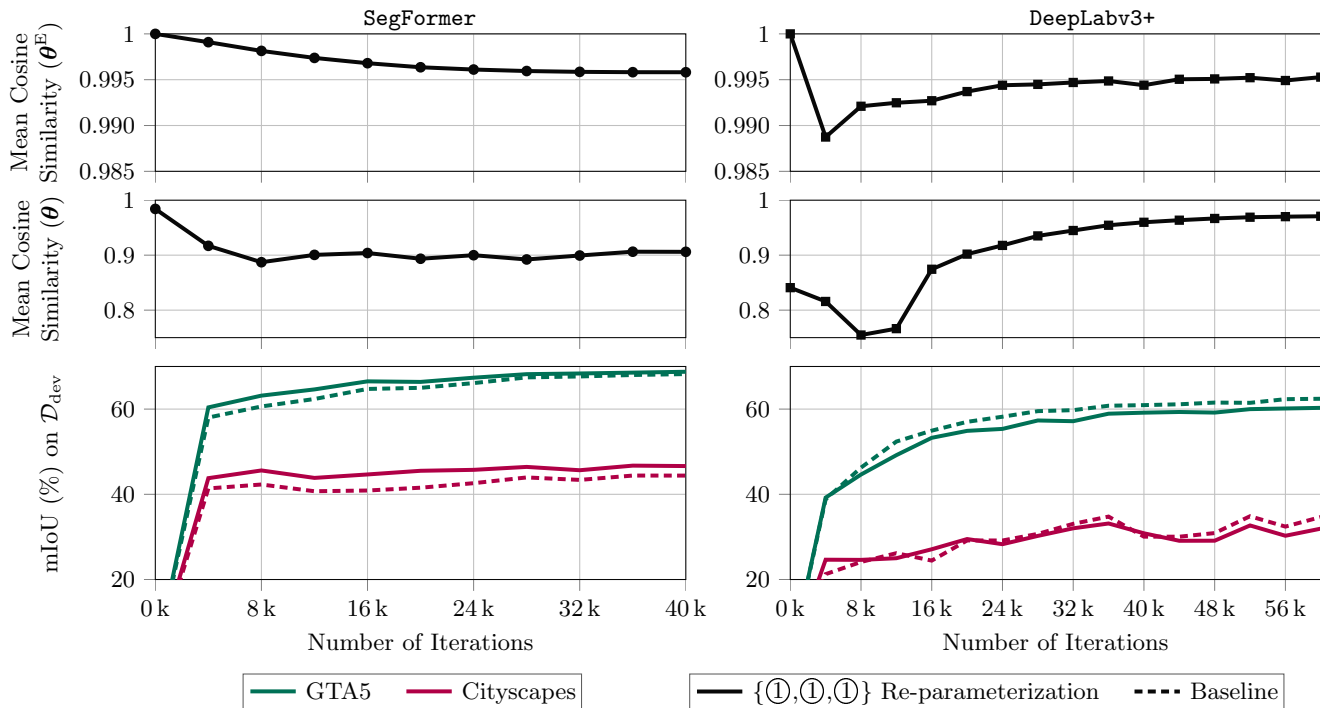


Figure 5. Comparison of **mean cosine similarity vs. mIoU performance** for SegFormer and DeepLabv3+ during training. The first row shows the mean cosine similarity for the encoder only ( $\theta^E$ ), the second row for the full network ( $\theta^E$ ). The mean cosine similarity is computed between three models. In the bottom row, the mIoU is given for the dev sets of GTA5 (green) and Cityscapes (red).

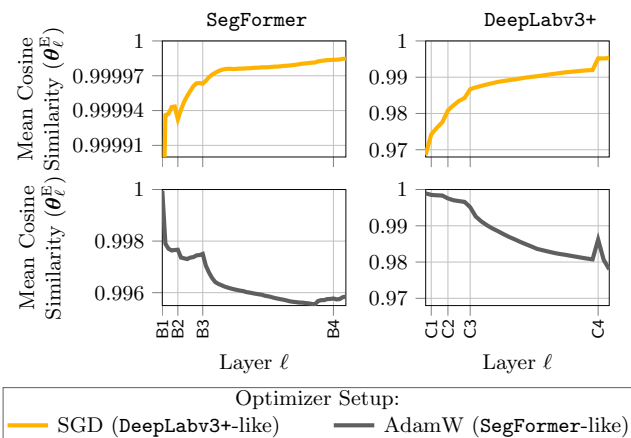


Figure 6. Comparison of the **layer-wise mean cosine similarity** for the encoder only ( $\theta_\ell^E$ ). Shown are results for the SegFormer (left) and DeepLabv3+ (right) architectures, which were trained with the standard DeepLabv3+ or SegFormer optimizer setup, shown in gray and yellow, respectively. The mean cosine similarity is computed between three models. For the purpose of clarity, we only indicate the individual network blocks ( $B_b$  for SegFormer,  $C_c$  for DeepLabv3+) on the x axis.

ure 8). For the DeepLabv3+, we indicate the convolutional blocks, as defined by He et al. [48], by  $C_c$  with  $c$

being the block index. *It can be seen that the choice of optimizer has a significant effect on the layer-wise cosine similarity.* For the standard DeepLabv3+ optimizer setup with SGD, the cosine similarity for both network architectures is higher in deeper layers and lower in earlier layers. In contrast, when the standard SegFormer optimizer setup with AdamW is employed, the cosine similarity is highest for earlier layers and drops for deeper layers. This specific property might be important for a well-performing encoder re-parameterization. As already shown in Table 4, this optimizer setup (AdamW [24]) also allows the DeepLabv3+ to improve over its baseline performance. Accordingly, we used the AdamW optimizer for our ReVT method in the main paper.

## D. Additional Ablation Studies

In this section, we will investigate the weighting of the base models and compare the ReVT re-parameterization w.r.t. re-parameterized network parts, layers, and the number of base models. Afterwards, we evaluate different base model augmentations and optimizer methods during training to design our final ReVT.

**Weighting of networks:** In Figure 7 we depict multiple possible weighting combinations for three models with the best combination (marked with a blue circle) achieving an mIoU of 47.68%, while the uniform re-parameterization

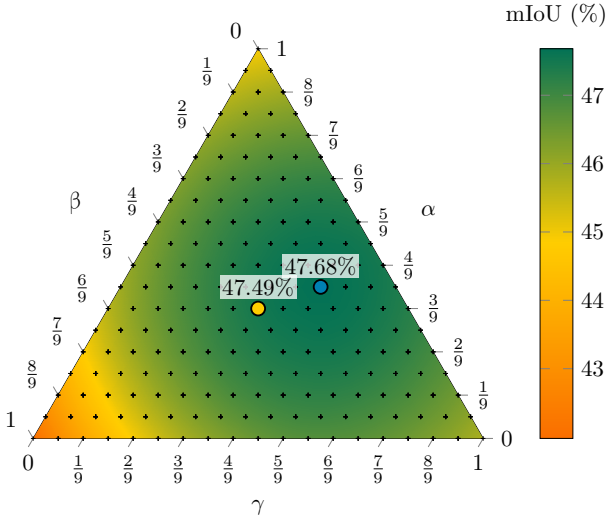


Figure 7. Ternary plot showing the performance (mIoU (%)) of three baseline models  $\{\textcircled{1}, \textcircled{1}, \textcircled{1}\}$  and multiple weight combinations  $(\alpha, \beta, \gamma)$ . The mIoU is calculated by a re-parameterization, where the parameters of the three models are weighted by the values of  $\alpha$ ,  $\beta$ , and  $\gamma$ , respectively. The **training** of the base models (SegFormer) was performed on the synthetic **GTA5** training set ( $\mathcal{D}^S = \mathcal{D}_{\text{train}}^{\text{GTA5}}$ ). The **evaluation** is performed on the **Cityscapes development set** ( $\mathcal{D}^T = \mathcal{D}_{\text{dev}}^{\text{CS}}$ ). The center of the plot ( $\alpha = \beta = \gamma = \frac{1}{3}$ ) corresponds to a uniform encoder re-parameterization.

(all models weighted with  $\frac{1}{3}$ , marked with a yellow circle) achieves an mIoU of 47.49%. It can be seen that the weighting of the individual models is actually quite insensitive, which is why we decide to use the simple variant of the uniform encoder re-parameterization (i.e., weights  $\frac{1}{3}$ ).

**ReVT vs. ensembles:** In Table 10 we compare the ReVT and a network ensemble for different combinations of training settings. It can be seen that the ReVT method outperforms the network ensemble not only for the combination of three baseline models  $\{\textcircled{1}, \textcircled{1}, \textcircled{1}\}$ , as already shown in Figure 4, but also for all other tested base model combinations  $\{\textcircled{u}_1, \textcircled{u}_2, \textcircled{u}_3\}$  on the real test\* sets. However, the network ensemble is slightly better in the synthetic source domain ( $\mathcal{D}_{\text{dev}}^{\text{GTA5}}$ ), which has little relevance for real-world applications. The same applies to the base model combination  $\{\textcircled{5}, \textcircled{5}, \textcircled{5}\}$ , where the ensemble performs slightly better on the SYNTHIA dataset ( $\mathcal{D}_{\text{dev}}^{\text{SYN}}$ ). The overall best performance for each dataset is highlighted in light green. It can be seen that the ReVT method achieves top performance for each dataset and is even on par with the ensemble on the source dataset ( $\mathcal{D}_{\text{dev}}^{\text{GTA5}}$ ). In general, once again, the ReVT  $\{\textcircled{1}, \textcircled{4}, \textcircled{6}\}$  seems to be a strong ReVT, generalizing well to unseen datasets.

Table 10. Performance (mIoU (%)) of a **network ensemble** vs. the **ReVT** for different base model combinations. The **training** of the base models (SegFormer) was performed on the **GTA5** ( $\mathcal{D}^S = \mathcal{D}_{\text{train}}^{\text{GTA5}}$ ) dataset. The **evaluation** is performed on the **GTA5** and **SYNTHIA development sets** and on the **test\* data** of various real-world target datasets ( $\mathcal{D}^T = \mathcal{D}_{\text{test}*}$ ). Reported is the mean value over the respective number of employed base models. Best result for each base model combination in bold face, overall best performance per dataset is highlighted in light green.

Base Models	Method	mIoU (%) on				
		$\mathcal{D}_{\text{dev}}^{\text{GTA5}}$	$\mathcal{D}_{\text{dev}}^{\text{SYN}}$	$\mathcal{D}_{\text{test}*}^{\text{CS}}$	$\mathcal{D}_{\text{test}*}^{\text{BDD}}$	$\mathcal{D}_{\text{test}*}^{\text{MV}}$
$\{\textcircled{1}, \textcircled{1}, \textcircled{1}\}$	Ensemble	<b>68.8</b>	34.6	46.9	44.8	48.0
	ReVT	68.6	<b>35.5</b>	<b>49.3</b>	<b>45.3</b>	<b>49.3</b>
$\{\textcircled{2}, \textcircled{2}, \textcircled{2}\}$	Ensemble	<b>69.2</b>	33.1	43.8	43.9	46.6
	ReVT	69.1	<b>34.1</b>	<b>44.9</b>	<b>44.1</b>	<b>47.6</b>
$\{\textcircled{3}, \textcircled{3}, \textcircled{3}\}$	Ensemble	<b>69.7</b>	33.8	43.8	42.6	47.3
	ReVT	<b>69.7</b>	<b>35.0</b>	<b>45.7</b>	<b>43.5</b>	<b>48.8</b>
$\{\textcircled{4}, \textcircled{4}, \textcircled{4}\}$	Ensemble	<b>65.9</b>	<b>36.8</b>	47.5	47.4	52.6
	ReVT	65.7	36.2	<b>48.8</b>	<b>47.5</b>	<b>53.2</b>
$\{\textcircled{5}, \textcircled{5}, \textcircled{5}\}$	Ensemble	<b>68.6</b>	35.1	47.5	45.4	50.4
	ReVT	<b>68.5</b>	<b>35.9</b>	<b>48.6</b>	<b>45.9</b>	<b>51.2</b>
$\{\textcircled{6}, \textcircled{6}, \textcircled{6}\}$	Ensemble	<b>65.0</b>	<b>37.0</b>	48.0	47.9	52.8
	ReVT	64.9	36.1	<b>49.7</b>	<b>48.5</b>	<b>53.5</b>
$\{\textcircled{4}, \textcircled{5}, \textcircled{6}\}$	Ensemble	<b>67.2</b>	35.1	48.1	47.3	51.6
	ReVT	<b>66.4</b>	<b>36.9</b>	<b>49.5</b>	<b>48.1</b>	<b>53.1</b>
$\{\textcircled{1}, \textcircled{4}, \textcircled{6}\}$	Ensemble	<b>68.5</b>	34.2	47.0	45.9	50.1
	ReVT	66.4	<b>37.3</b>	<b>50.0</b>	<b>48.0</b>	<b>52.8</b>

## E. ReVT with SYNTHIA as Source

In this section, we provide additional results for our method, when trained with the SYNTHIA dataset as source domain:  $\mathcal{D}^S = \mathcal{D}_{\text{train}}^{\text{SYN}}$ . In Table 11 we evaluate the various augmentation methods  $\textcircled{a}$  that were already evaluated for models trained on GTA5 ( $\mathcal{D}^S = \mathcal{D}_{\text{train}}^{\text{SYN}}$ ) in Section 5. In the lower part of the table we report some ( $M = 3$ ) combinations  $\{\textcircled{u}_1, \textcircled{u}_2, \textcircled{u}_3\}$  of these base models by our re-parameterization. The gray columns indicate our development sets ( $\mathcal{D}_{\text{dev}}$ ), where the light gray column is  $\mathcal{D}_{\text{dev}}^{\text{SYN}}$ . The OOD mean mIoU of  $\mathcal{D}_{\text{dev}}^{\text{GTA5}}$  and  $\mathcal{D}_{\text{dev}}^{\text{CS}}$  is shown in the dark gray columns. It can be seen in the upper part of Table 11 that the augmentation methods do not improve the performance as much as for models trained on GTA5. The best OOD mean performance is achieved with the baseline model  $\textcircled{1}$ . On the test\* mean the PixMix\* augmentation works best, followed by the combination of PixMix\* and the bilateral filter, and baseline model.

Although the individual augmentations do not perform as well for these models, the ReVT  $\{\textcircled{1}, \textcircled{4}, \textcircled{6}\}$ , which we

Table 11. Performance (mIoU (%)) of the SegFormer model (with an MiT-B5 encoder) using different domain generalization methods. **Training** was performed on the synthetic SYNTHIA ( $\mathcal{D}^S = \mathcal{D}_{\text{train}}^{\text{SYN}}$ ) dataset. **Evaluation** is performed on the **Cityscapes**, **GTA5**, and **SYNTHIA development sets** (gray columns) and on the **test\* data** of various real-world target datasets ( $\mathcal{D}^T = \mathcal{D}_{\text{test}^*}$ ). Reported is the mean mIoU  $\pm$  the standard deviation of  $M=3$  models with various image augmentations. For the ReVT, the mean  $\pm$  standard deviation is computed with one averaged encoder and the three associated decoders  $m \in \{1, 2, 3\}$ . For models trained on SYNTHIA, we evaluate over 16 classes, as is common practice [19]. Best results in bold face, second-best underlined.

Method performed:		mIoU (%) on							
		$\mathcal{D}_{\text{dev}}^{\text{SYN}}$	$\mathcal{D}_{\text{dev}}^{\text{GTA5}}$	$\mathcal{D}_{\text{dev}}^{\text{CS}}$	<b>OOD mean</b>	$\mathcal{D}_{\text{test}^*}^{\text{CS}}$	$\mathcal{D}_{\text{test}^*}^{\text{BDD}}$	$\mathcal{D}_{\text{test}^*}^{\text{MV}}$	<b>test* mean</b>
during training	Baseline ①	76.5 $\pm$ 0.1	42.8 $\pm$ 0.4	<b>44.3</b> $\pm$ 1.3	<b>43.5</b> $\pm$ 1.2	<b>45.1</b> $\pm$ 1.6	35.2 $\pm$ 1.4	<b>42.5</b> $\pm$ 0.9	<u>40.9</u> $\pm$ 4.4
	-PhotoAug ②	<u>77.3</u> $\pm$ 0.1	39.8 $\pm$ 0.6	41.4 $\pm$ 0.5	40.6 $\pm$ 0.9	41.6 $\pm$ 0.8	33.7 $\pm$ 1.0	40.8 $\pm$ 0.6	38.7 $\pm$ 3.6
	-PhotoAug, -Rand. Flip ③	<b>78.3</b> $\pm$ 0.0	40.7 $\pm$ 0.7	41.3 $\pm$ 0.3	41.0 $\pm$ 0.6	41.8 $\pm$ 0.2	34.3 $\pm$ 1.1	41.3 $\pm$ 0.3	39.1 $\pm$ 3.5
	+PixMix* [13] ④	73.8 $\pm$ 0.1	<b>43.1</b> $\pm$ 1.0	42.6 $\pm$ 1.7	42.8 $\pm$ 1.4	42.6 $\pm$ 2.2	<b>38.4</b> $\pm$ 0.8	<b>42.5</b> $\pm$ 0.6	<b>41.2</b> $\pm$ 2.4
	+Bilateral Filter (BF) [39] ⑤	76.0 $\pm$ 0.1	42.9 $\pm$ 0.9	43.2 $\pm$ 0.7	<u>43.1</u> $\pm$ 0.8	43.1 $\pm$ 0.9	36.0 $\pm$ 0.7	41.7 $\pm$ 0.4	40.3 $\pm$ 3.1
	+PixMix* [13] +BF [39] ⑥	72.3 $\pm$ 0.1	41.2 $\pm$ 0.6	<u>43.3</u> $\pm$ 0.4	42.2 $\pm$ 1.2	<u>43.0</u> $\pm$ 0.5	<u>38.0</u> $\pm$ 0.6	41.6 $\pm$ 0.3	<u>40.9</u> $\pm$ 2.2
after training	ReVT {①,①,①}	76.2 $\pm$ 0.1	42.3 $\pm$ 0.1	44.9 $\pm$ 0.4	43.6 $\pm$ 1.3	<u>45.8</u> $\pm$ 0.4	35.8 $\pm$ 0.2	43.6 $\pm$ 0.2	41.7 $\pm$ 4.3
	ReVT {②,②,②}	<u>76.9</u> $\pm$ 0.0	40.4 $\pm$ 0.2	42.2 $\pm$ 0.2	41.3 $\pm$ 1.0	42.6 $\pm$ 0.1	34.7 $\pm$ 0.3	42.0 $\pm$ 0.3	39.8 $\pm$ 3.6
	ReVT {③,③,③}	<b>78.0</b> $\pm$ 0.1	41.3 $\pm$ 0.6	41.9 $\pm$ 0.3	41.6 $\pm$ 0.6	42.5 $\pm$ 0.4	35.2 $\pm$ 0.3	42.7 $\pm$ 0.3	40.1 $\pm$ 3.5
	ReVT {④,④,④}	73.7 $\pm$ 0.1	<u>43.4</u> $\pm$ 0.1	44.1 $\pm$ 0.3	43.7 $\pm$ 0.4	44.3 $\pm$ 0.3	39.5 $\pm$ 0.3	<u>44.0</u> $\pm$ 0.3	42.6 $\pm$ 2.2
	ReVT {⑤,⑤,⑤}	75.7 $\pm$ 0.0	<b>44.1</b> $\pm$ 0.7	44.4 $\pm$ 0.3	<b>44.2</b> $\pm$ 0.6	44.5 $\pm$ 0.3	37.1 $\pm$ 0.3	43.0 $\pm$ 0.2	41.5 $\pm$ 3.2
	ReVT {⑥,⑥,⑥}	72.2 $\pm$ 0.1	42.4 $\pm$ 0.2	44.4 $\pm$ 0.2	43.4 $\pm$ 1.0	44.3 $\pm$ 0.2	38.9 $\pm$ 0.2	42.9 $\pm$ 0.0	42.0 $\pm$ 2.3
	ReVT {④,⑤,⑥}	74.0 $\pm$ 0.6	43.2 $\pm$ 0.4	<u>45.0</u> $\pm$ 0.4	<u>44.1</u> $\pm$ 0.9	45.1 $\pm$ 0.4	<u>39.6</u> $\pm$ 0.4	<u>44.0</u> $\pm$ 0.2	<u>42.9</u> $\pm$ 2.4
	ReVT {①,④,⑥}	74.1 $\pm$ 0.6	42.7 $\pm$ 0.3	<b>45.7</b> $\pm$ 0.5	<b>44.2</b> $\pm$ 1.5	<b>46.3</b> $\pm$ 0.3	<b>40.3</b> $\pm$ 0.5	<b>44.8</b> $\pm$ 0.1	<b>43.8</b> $\pm$ 2.6

already identified as our best ReVT in Section 5, provides both top OOD mean (44.2%) and test\* mean (43.8%) performance. Again, second-best results are achieved with the ReVT {④,⑤,⑥}. Additionally, the ReVT {⑤,⑤,⑤} is on par with the ReVT {①,④,⑥} for the OOD mean performance when trained on SYNTHIA.

In the following, we compare also against prior art that have also been evaluated with SYNTHIA as source domain. Again, we choose the ReVT {①,④,⑥} and ReVT {④,⑤,⑥} for the comparison with prior art. The results are shown in Table 12. In contrast to the models trained on GTA5, for models trained on SYNTHIA, the ReVT {①,④,⑥} does not always reach the top BM mean performance. Similar to the GTA5-trained models, the performance of both ReVT variants remains slightly behind that of the baseline for synthetic source domain data ( $\mathcal{D}_{\text{dev}}^{\text{SYN}}$ ), which, however, has little relevance for practical real-world applications.

For the small (group 1) and mid-sized (group 2) models, the ReVT {④,⑤,⑥} yields a slightly better performance of 45.79% vs. 45.44% (baseline: 44.09%) and 48.99% vs. 48.84% (baseline: 46.72%), respectively. For the large models (group 3), the ReVT {①,④,⑥} yields the best performance with a BM mIoU of 49.64% (base-

line: 48.42%). In summary, on the benchmark (BM) data, our proposed SYNTHIA-trained ReVT models achieve an mIoU improvement of +1.2% absolute (large models) to +1.7% absolute (small models).

It should be noted that no prior work reported on all datasets necessary for the benchmark (BM) mean when trained with SYNTHIA as source domain. All of our ReVTs improve on the prior art for the reported domains. Only for the smallest models in group 1 the SAN+SAW method [30] achieves a higher mIoU on the BDD dataset (best prior art: 35.42% vs. ours: 35.18%). For the mid-sized models we already improve on this domain (best prior art: 37.40% vs. ours: 38.73%), and interestingly significantly excel the SAN+SAW method (ours: 38.73% vs. SAN+SAW: 35.98%).

## F. SegFormer Block Diagrams

In Section 5 we investigated the effect of the re-parameterization on different network parts (cf. Table 3) and block or layer types (cf. Table 5). To give the reader a better idea of how the network is structured and where the individual block and layer types are located in the network, an hierarchically illustrated overview of the SegFormer architecture with an MiTB5 encoder is given in Figures 8, 9,

Table 12. Performance (mIoU (%)) of various domain generalization methods employing different segmentation networks, sorted into three performance groups. **Training** was performed on the synthetic **SYNTHIA** ( $\mathcal{D}^S = \mathcal{D}_{\text{train}}^{\text{SYN}}$ ) dataset. The results marked with  $^\circ$  are cited from [20] and with  $*$  are cited from the respective paper. All results without any identifier are simulated. **Evaluation** is performed on the **SYNTHIA** and **GTA5 development sets** and on the **test\* data** of various real-world target datasets ( $\mathcal{D}^T = \mathcal{D}_{\text{test}*}$ ). BM means benchmark. For our simulations we report mean values over three runs with different seeding. For models trained on SYNTHIA, we evaluate over 16 classes, as is common practice [19]. Best performance per group in bold face, second best underlined.

Enc.	Method	$ \theta $ ( $\cdot 10^6$ )	Single Source	Frame Rate [fps]	mIoU (%) on								
					$\mathcal{D}_{\text{test}*}^{\text{CS}}$	$\mathcal{D}_{\text{test}*}^{\text{BDD}}$	$\mathcal{D}_{\text{test}*}^{\text{MV}}$	$\mathcal{D}_{\text{dev}}^{\text{SYN}}$	$\mathcal{D}_{\text{dev}}^{\text{GTA5}}$	$\mathcal{D}_{\text{test}*}^{\text{ACDC}}$	$\mathcal{D}_{\text{test}*}^{\text{KIT}}$	BM mean	
Group 1	ResNet-50	Baseline $^\circ$	49.6	✓	7.9	28.36	25.16	27.24	-	-	-	-	-
		DRPC $^\circ$ [44]	49.6	✗	8.3	35.65	31.53	32.74	-	-	-	-	-
		SAN+SAW* [30]	25.6	✓	8.1	38.92	<b>35.42</b>	34.52	-	29.16	-	-	-
	MiT-B2	Baseline	27.4	✓	<b>12.0</b>	39.71	29.76	38.37	<b>74.78</b>	37.83	26.16	<u>35.18</u>	44.09
		Ours: ReVT {④,⑤,⑥}	27.4	✓	<b>12.0</b>	<b>41.09</b>	<u>35.18</u>	<u>40.21</u>	<u>71.59</u>	<b>40.88</b>	<b>30.39</b>	34.64	<b>45.79</b>
		Ours: ReVT {①,④,⑥}	27.4	✓	<b>12.0</b>	<u>40.91</u>	34.53	<b>40.44</b>	71.45	<u>39.87</u>	<u>30.13</u>	<b>35.29</b>	<u>45.44</u>
Group 2	ResNet-101	Baseline $^\circ$	68.6	✓	7.9	29.67	25.64	28.73	-	-	-	-	-
		DRPC $^\circ$ [44]	68.6	✗	5.3	37.58	34.34	34.12	-	-	-	-	-
		FSDR* [14]	68.6	✗	5.3	40.80	37.40	39.60	-	-	-	-	-
		SAN+SAW* [30]	44.6	✓	5.3	40.87	35.98	37.26	-	30.79	-	-	-
	MiT-B3	Baseline	47.2	✓	<b>10.7</b>	42.43	33.33	40.47	<b>75.82</b>	41.53	29.73	35.91	46.72
		Ours: ReVT {④,⑤,⑥}	47.2	✓	<b>10.7</b>	<b>45.26</b>	<b>38.73</b>	<u>42.86</u>	73.12	<b>44.99</b>	<b>35.27</b>	<b>36.42</b>	<b>48.99</b>
Ours: ReVT {①,④,⑥}		47.2	✓	<b>10.7</b>	<u>44.97</u>	<u>38.65</u>	<b>43.00</b>	<u>73.16</u>	<u>44.42</u>	<u>35.16</u>	<u>36.31</u>	<u>48.84</u>	
Group 3	MiT-B5	Baseline	84.7	✓	<b>9.7</b>	45.07	35.19	42.51	<b>76.49</b>	<u>42.82</u>	30.81	37.02	48.42
		Ours: ReVT {④,⑤,⑥}	84.7	✓	<b>9.7</b>	<u>45.08</u>	<u>39.62</u>	<u>43.99</u>	73.96	<b>43.25</b>	<u>35.12</u>	<u>37.20</u>	<u>49.18</u>
		Ours: ReVT {①,④,⑥}	84.7	✓	<b>9.7</b>	<b>46.28</b>	<b>40.30</b>	<b>44.76</b>	<u>74.11</u>	42.74	<b>35.75</b>	<b>37.86</b>	<b>49.64</b>

10, 11, and 12.

## G. Discussion of Limitations

Although modern methods for domain generalization provide good performance on completely unseen real data (after training on synthetic data), the performance still remains behind that of modern methods for unsupervised domain adaptation (UDA) [47,49]. Such a comparison, however, is not entirely fair, since UDA methods employ unlabeled data from a target domain (typically Cityscapes) during the training process, which we intentionally avoid in domain generalization. Nevertheless, it should be noted that better performance on a specific target domain can be achieved, if samples from this domain are available during training.

Our proposed method cannot be applied advantageously to any already trained model, since the optimizer choice has a significant impact on the performance. To be fair, however, this is the case with all prior art methods as well. Most of them additionally extend the training process considerably, far beyond the choice of the optimizer [5, 14, 20, 30, 44].

## H. Discussion of Ethical Implications

Although well generalizing semantic segmentation has many civilian applications that provide great value to society, e.g., automated driving, robotics, and medical applications, this technology can also be used for military and surveillance applications. Research on better generalizing methods may also indirectly contribute to the improvement of these applications.

Another aspect to consider are biases in the employed datasets. Three of the five real datasets (Cityscapes, ACDC, KITTI) were captured in Central Europe, one in the USA (BDD100k), and only one contains data from all over the world (Mapillary Vistas). This may lead to biases regarding different ethnicities in the data, which were not investigated further in this paper. For the reported results on improved generalization from synthetic to real data, the biases may be negligible, but should be considered for possible real-world applications.



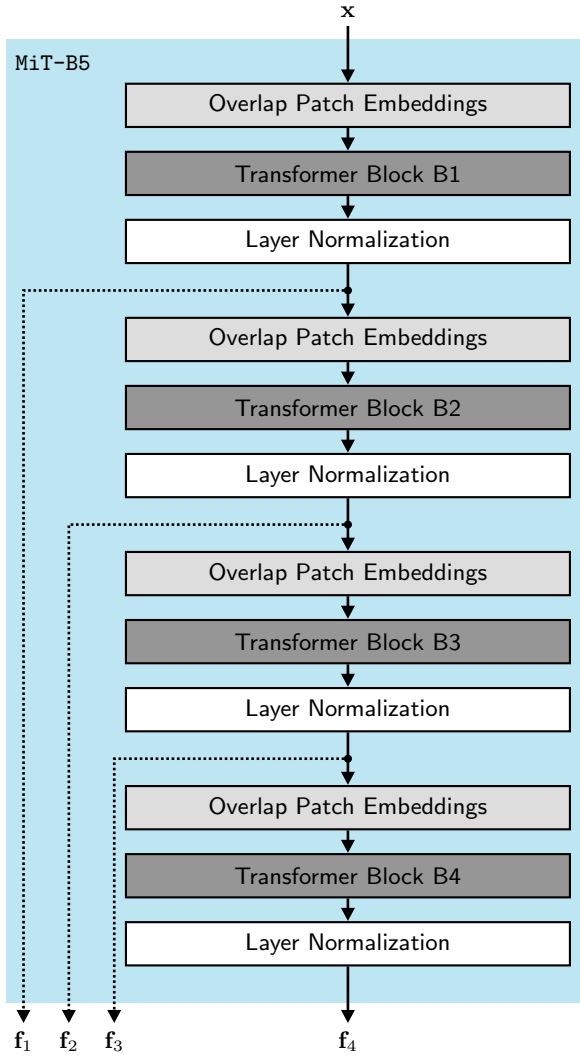


Figure 8. Overview of the MiT-B5 encoder that is employed by the largest SegFormer model. This is the standard encoder employed in the segmentation model (cf. Figure 2).

**Additional References**

- [47] Nikita Araslanov and Stefan Roth. Self-Supervised Augmentation Consistency for Adapting Semantic Segmentation. In *Proc. of CVPR*, pages 15384–15394, virtual, June 2021.
- [48] Kaiming He, Xiangyu Zhang, Shaoqing Ren, and Jian Sun. Deep Residual Learning for Image Recognition. In *Proc. of CVPR*, pages 770–778, Las Vegas, NV, USA, June 2016
- [49] Lukas Hoyer, Dengxin Dai, and Luc Van Gool. DAFormer: Improving Network Architectures and Training Strategies for Domain-Adaptive Semantic Segmentation. In *Proc. of CVPR*, pages 9924–9935, New Orleans, LA, USA, June 2022

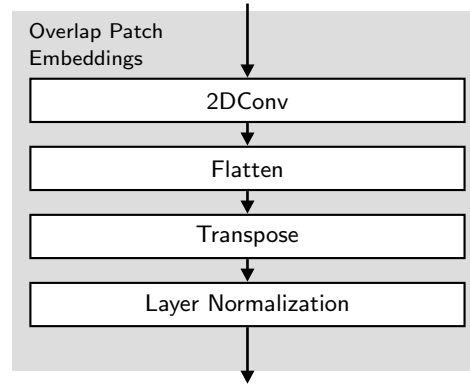


Figure 9. Overview of the overlap patch embeddings block that is employed in the MiT encoder (cf. Figure 8 for MiT-B5).

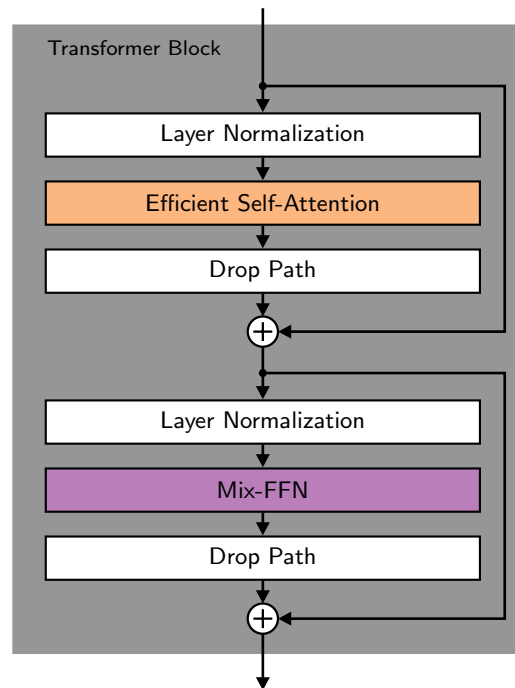


Figure 10. Overview of the transformer block that is employed in the MiT encoder (cf. Figure 8 for MiT-B5).

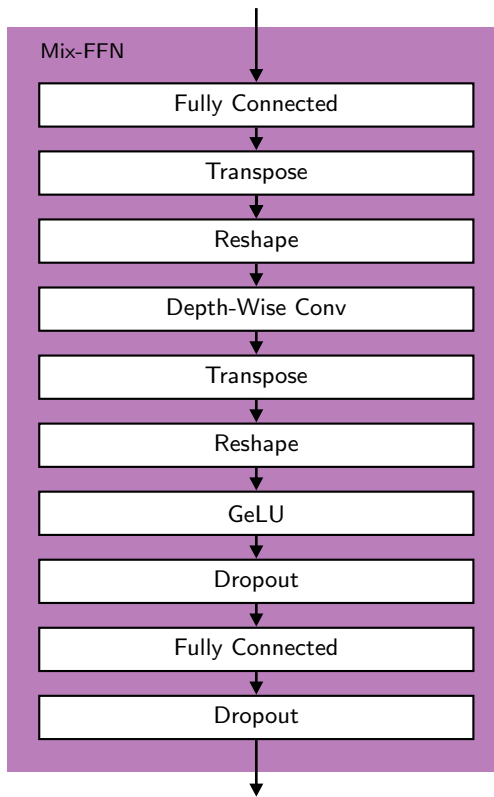


Figure 11. Overview of the Mix-FFN block that is employed in the transformer block (cf. Figure 10).

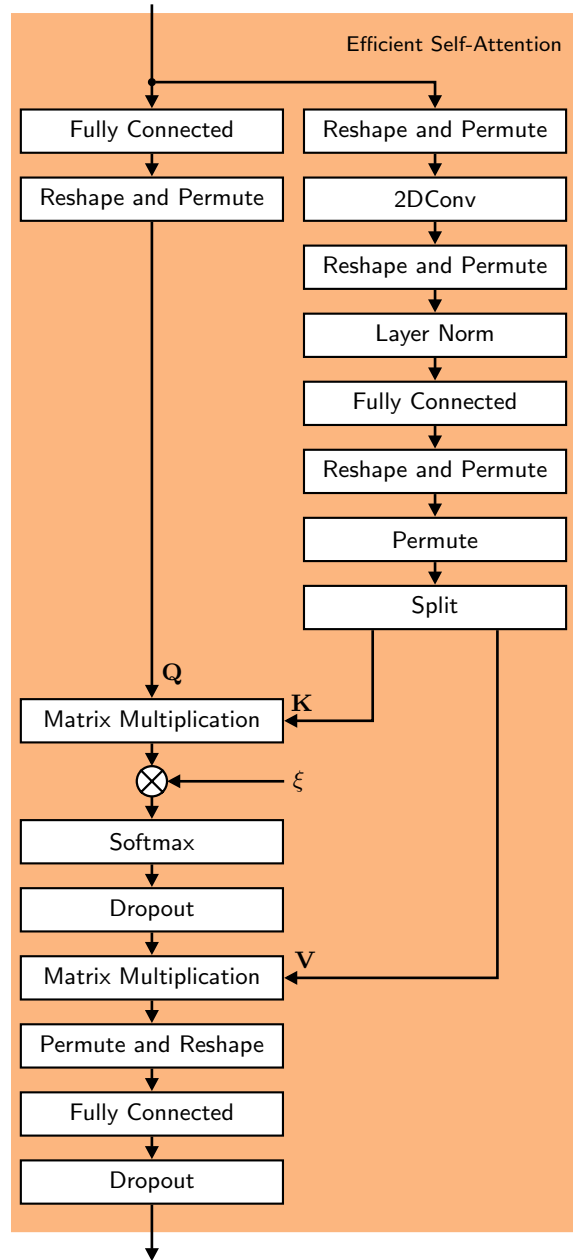


Figure 12. Overview of the efficient self-attention block that is employed in the transformer block (cf. Figure 10). The fixed scaling factor  $\xi$  is a hyperparameter and block-dependent.